EGG-2445
DE-1618-7

Geothermal Injection Technology Program

Annual Progress Report: FY-85

Prepared by:
Idaho National Engineering Laboratory
and
University of Utah Research Institute

F O R M A L R E P O R T

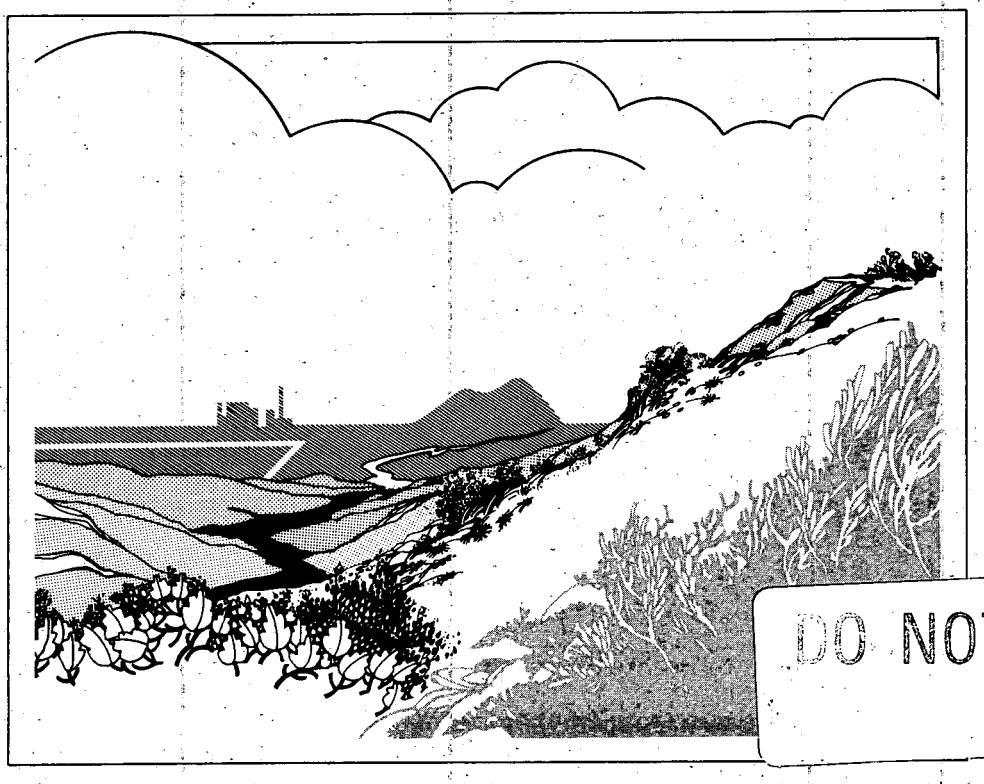

EG&G Idaho

Work performed under
DOE Contract No. DE-AC07-76ID01570

Idaho National Engineering Laboratory

Managed by the U.S. Department of Energy

DISCLAIMER

Printed in the United States of America

Available from
National Technical Information Service
U.S. Department of Commerce
5285 Port Royal Road
Springfield, VA 22161
NTIS Price Codes: Printed Copy A03
Microfiche A01

EGG-2445
Distribution Category: UC-66a

EGG--2445

DE86 008319

GEOTHERMAL INJECTION TECHNOLOGY PROGRAM

ANNUAL PROGRESS REPORT: FY-85

Prepared by:

Idaho National Engineering Laboratory
and
University of Utah Research Institute

Published February 1986

Prepared for the
U.S. Department of Energy
Idaho Operations Office
Under DOE Contract No. DE-AC07-76ID01570

EXECUTIVE SUMMARY

The injection of spent geothermal fluids has been identified as one of the primary technical concerns currently facing geothermal developers. Injection is used not only to dispose of the large volumes of spent geothermal fluids associated with power generation and direct use developments, but also to offset reservoir depletion and reduce the risk of subsidence by maintaining reservoir pressures.

Injection can result, however, in thermal breakthrough to production wells, loss of injectivity due to chemical interactions in the reservoir, scaling and corrosion in piping and wells, aquifer contamination, and increased seismicity. Assessment of these thermal, chemical, and physical impacts cannot be accomplished using standard reservoir engineering techniques. Solutions to these technical problems require long-term, potentially high-risk research.

During the past three years, the University of Utah Research Institute (UURI) and the Idaho National Engineering Laboratory (INEL) have been conducting injection research and testing sponsored by the U.S. Department of Energy, Division of Geothermal and Hydropower Technologies. Unique analytical techniques and capabilities have been developed at both institutions in support of injection research. The interdisciplinary staff of earth scientists, physicists and engineers, and the research facilities dedicated to this injection research represent a broad range of technological resources and experience.

This report presents a summary of the UURI and INEL injection research activities conducted during FY-1985. The primary objective of the research programs is to develop a better understanding of the migration and impact of fluids injected in geothermal reservoirs. Laboratory testing, field investigations, and numerical simulations provide the basis for the research.

The 1985 injection research program at UURI emphasized the development and application of tracers for geothermal applications. Tracers can be used to monitor the migration of injected fluids and provide a reference to quantify chemical changes resulting from injection. Few tracers are presently available which have been used in a geothermal environment and little is known about their thermal stability and chemical reactivity.

The UURI program includes determining tracer stability, developing and testing new tracers, and field testing to confirm tracer behavior under actual reservoir conditions. The objective is to develop and test the application of tracers which are nonhazardous, stable, and conservative in high-temperature environments, and which provide the ability to independently monitor multiple wells in a geothermal wellfield.

Two categories of tracers were tested at UURI this year, fluorescein dyes and fluorinated and sulfonated hydrocarbons. Stabilizing and destabilizing factors were investigated in tests of fluorescein at temperatures up to 200°C. Stability tests of the fluorinated and sulfonated hydrocarbons showed four of the five species tested were more stable than organic dyes currently in use by the geothermal industry. These hydrocarbon tracers are available in a number of species providing the added ability to tag individual wells in a wellfield.

Continued tests of the fluorinated and sulfonated hydrocarbons are planned by UURI to determine their thermal stabilities and to assess their properties at high temperatures. Additional high-temperature tests of fluorescein will be conducted in various geothermal brines to further evaluate stabilizing influences.

The objective of the INEL injection research program is to develop a sound theoretical understanding of the fundamental processes that control mass, heat, and solute transport in fractured reservoirs in order to understand how geothermal reservoirs respond to fluid injection. Analytical and testing techniques are developed based on these processes which can be used to track injected fluids and to evaluate their impact.

The FRactured media—Advanced Continuous Simulation Language (FRACSL) code has been developed as a tool to aid in the investigation of flow and transport in porous media, discrete fractures, and dual-permeability reservoirs. The code's dual-permeability capability allows analyses of fluid migration in fractured reservoirs with significant matrix permeability that can impact fluid transport and heat transfer. The FRACSL code has been validated against analytical solutions for flow and transport in porous media. Correlation of testing conducted at the East Mesa geothermal field has demonstrated the utility of the code.

Physical models are being used to study the dispersion phenomenon in fractures under controlled conditions, where observation can help increase the understanding of fluid and tracer transport processes. The models also provide a means to validate computer codes that simulate flow and transport in fracture networks and allow evaluation of field test procedures under known reservoir conditions. This year, physical model testing was oriented towards validating the tracer tracking algorithm used in FRACSL, and developing a better understanding of transport processes in fractures. The former activity has shown that particle tracking has many advantages over equation solution methods for simulating solute transport. The latter activity has provided important insight into how to design future tests of fracture systems. Laboratory tests using the discrete fracture network model were also used to demonstrate the significance of density effects in fluid transport. Preliminary simulations were made with a dual-permeability physical model which allows advective and diffusive transfer of fluid between fractures and matrix.

Future INEL research efforts will continue development of techniques to evaluate and predict the impact of injection on geothermal reservoirs. Primary emphasis will be placed on dual-permeability physical model tests, further development and validation of the FRACSL code, and cooperative injection tests with industry.

CONTENTS

NOMENCLATURE

(L = length, t = time, m = mass)

a	Fracture height for rectangular channels (L)
ANORM	Random variable with mean 0 and variance 1
b	Fracture aperture (L)
C	Concentration (m/L^3)
D_m	Molecular diffusion coefficient (L^2/t)
f_r	Friction factor
g	Acceleration of gravity (L/t^2)
k	Hydraulic conductivity (L/t)
M	Mass (m)
Q	Mass flow rate (m/t)
QABS	Position of a particle on a cumulative discharge scale for calculating transfer through a junction (L^3/t)
Q_f	Fracture discharge (L^3/t)
Q_p	Discharge between a particle at position y in a fracture and the adjacent fracture wall (L^3/t)
r	Radial distance (L)
t	Time (t)
V	Volume (L^3)
v	Local flow velocity (L/t)
$\bar{v}$	Average flow velocity (L/t)
v_c	Peak flow velocity along the centerline of a fracture (L/t)
x	Linear distance along fracture (L)
y	Distance across width of fracture (L)
z	Thickness (L)
S	Specific storage ($L^3/L \cdot L^2$)
μ	Viscosity ($m/L \cdot t$)

ρ	Density (m/L^3)
ϕ	Head (L)
η	Fractional position of particle in fracture
ξ	Porosity

GEOTHERMAL INJECTION TECHNOLOGY PROGRAM

1. INTRODUCTION

The overall objective of the Injection Technology Research Program at the University of Utah Research Institute (UURI) and the Idaho National Engineering Laboratory (INEL) is to develop a better understanding of fluid migration in fractured geothermal systems during injection. This understanding will be used to predict the fate of injected fluids and to improve field testing and data interpretation procedures.

Breakthrough of fluids to production wells can cause loss of enthalpy and increased scale deposition. While injected fluids may, with time, reheat in the reservoir, increasing dissolved solids content from previous flashes may eventually cause operational difficulties. Injected fluids may also move towards potable water resources causing environmental problems. Water/rock interactions that affect reservoir permeability must be understood to protect against loss of injection capacity. Innovative testing and data analysis methods can lead to an improved understanding of a geothermal reservoir, resulting in more efficient reservoir development and lower development risk.

The INEL/UURI Injection Technology Research Program combines laboratory experimentation, computer simulation, and field testing in the study of injected fluid migration. Methods of interpreting data are refined by relating observable phenomena (pressure response, fluid temperature, tracer breakthrough) to reservoir characteristics. Parametric studies can be performed using numerical simulation codes to determine the sensitivity of measurable parameters to changes in reservoir conditions. Codes are not only verified against analytical solutions, but are validated using laboratory models. The laboratory validation step provides assurance that the codes deal with the important transport processes properly.

1.1 Task 1: Fundamental Transport Processes

A sound theoretical understanding of the processes that control mass, heat, and solute transport through fractured rocks is necessary to understand how geothermal reservoirs will respond to fluid injection. Data analysis methods must incorporate this basic knowledge to provide insights into a geothermal reservoir. Laboratory models are used to collect data under controlled conditions. Simulation codes are improved by validation against these well-defined laboratory systems by making the computer algorithms more realistic. This validation step aids in separating uncertainty in code parameters from uncertainty in reservoir configuration.

In previous years, the transport algorithm for fractures was developed and a simple single fracture code written. The algorithm was verified against analytical solutions and validated against laboratory data. The FRactured media—Advanced Continuous Simulation Language (FRACSL) reservoir code currently uses this approach to tracer transport. The flow and transport components of FRACSL have been validated using a laboratory fracture network. A good match between the laboratory data and the FRACSL simulations was obtained. These previous laboratory and simulation studies have dealt with discrete fractures in impermeable matrix materials.

Because of the uncertainty concerning how solutes are transferred through fracture junctions, laboratory and computer simulation studies have been conducted to study this phenomenon. An algorithm for transferring tracer particles through junctions has been incorporated into the FRACSL code. This algorithm is based on streamline flow through junctions under laminar flow conditions. Some transfer of tracer across streamlines can occur by molecular diffusion, which is also included in the algorithm. Laboratory studies were conducted using the plexiglas fracture network to evaluate the fracture junction transfer function of FRACSL. Section 2 presents a detailed discussion of the mechanics of the FRACSL junction calculation, the laboratory validation experiments, and the range of conditions under which assumptions about transport through fracture systems are valid.

1.2 Task 2: Data Interpretation Tools

The objective of this task is to develop tools that can be used to interpret pressure, temperature, or tracer data obtained from testing geothermal reservoirs. Data interpretation tools are based on either analytical solutions to an idealized reservoir configuration (type-curve matching) or on distributed parameter simulation techniques. Because of the complexity of fractured, dual-permeability geothermal reservoirs, the INEL program emphasizes the latter approach. By adding the capability to match tracer response curves to the ability to match pressure and temperature data, additional information on reservoir conditions can be obtained.

Because of the complexity of fractured geothermal reservoirs, it is not possible to simulate the entire reservoir deterministically. That is, there are too many fractures to incorporate all explicitly into the simulation, and there is too little information on the individual fractures. Therefore, statistical descriptions of the fracture system are first generated, and an equivalent continuum used to describe these fractures. Only the major fractures are explicitly simulated in the model. The continuum portion of the reservoir may have considerable flow; therefore, this type of system cannot be simulated using a dual-porosity approach. One goal of the INEL program is to provide a code that can deal with flow through both the explicitly simulated fractures, and the complex fracture network that makes up the bulk of the reservoir.

Section 3 gives a status report on the FRACSL code. The first part of the report details the capabilities of the code and the modifications and improvements made to the code during FY-85. The latter part of the section details the code validation and verification work. The validation of the code is a critical step to providing assurance that quality results will be obtained when using the code.

1.3 Task 3: Tracer Development and Geochemistry

The full effect of injecting a relatively cool, supersaturated fluid into a geothermal reservoir cannot be modeled by just measuring the variables of temperature and pressure, which is the normal procedure for reservoir modeling. To effectively model injection, specific packets of fluid must be traced underground, and the temperature, pressure, timing, and saturation with respect to mineral phases must be monitored.

Tracers can be used to monitor the movement of groundwaters and geothermal fluids, and can be used as a reference to quantify changes in fluid chemistry as a result of injection. Despite their potential importance to the geothermal operator, very few tracers are presently available. Little is known about their stability or behavior at the elevated temperatures that typify geothermal resources suitable for electric power generation. During the past two years UURI has been involved in tracer research and testing. Their approach involves:

1. Determining the stability of tracers in current use by laboratory measurements
2. Developing and testing new tracer species, and
3. Performing field tests to determine tracer stabilities under actual reservoir conditions.

Section 4 discusses details of laboratory research conducted on developing new tracers. The sulfonated and fluorinated hydrocarbons are a promising new class of tracers. They appear to exhibit good thermal stability and, because of the wide range of compositions, could be used to trace many wells simultaneously. Geochemical interaction studies using tracers have been used to evaluate the quantity of water/rock interactions during field testing at the East Mesa geothermal field.

1.4 Task 4: Field Testing

An important component in the Department of Energy Geothermal Injection Technology Program is the validation of analytical and simulation techniques with field tests. These tests demonstrate the utility and constraints of techniques developed by research participants and also provide effective technology transfer to the geothermal industry.

Negotiations are currently underway with several geothermal developers to allow cooperative injection field tests in fractured or complex reservoirs during 1986. Researchers from UURI, INEL,

Stanford, the Lawrence Livermore National Laboratory and the Lawrence Berkeley Laboratory will participate in the tests.

Testing and analytical techniques which are included in the field testing program include single well and well-to-well tracer tests to provide data on heat transfer and heat extraction efficiency, transport of injected fluids, reservoir parameters, dispersion characteristics, and water-rock and water-water chemical interactions. The analytical data will be modeled with simulation techniques to predict thermal breakthrough and to evaluate the potential for formation plugging. New techniques which have been developed to interpret nonisothermal transient injection test data will be evaluated. Geophysical methods which can potentially provide information about the direction, depth, and rate of fluid migration will also be tested. Candidate methods which are being developed for this application include microseismic monitoring, self-potential surveys, multiborehole electrical imaging, repeat borehole gravity surveys, and passive pressure response (earth-tide and barometric fluctuations). Application of these techniques will depend on the particular reservoir characteristics of the test sites.

1.5 Task 5: Demonstration and Technology Transfer

The objective of this task is to demonstrate the effectiveness of various testing methods using simulation capabilities, and to transfer capabilities to the geothermal industry. Interaction with industry will strengthen the DOE program by encouraging industry support and soliciting feedback from industry on the utility of new developments.

1.6 Summary

The major advancements of the Injection Technology Research Program at INEL and UURI fall into three areas:

1. Development of conservative tracers
2. Further understanding of fundamental transport processes in fracture systems
3. Refinement of the FRACSL code for interpretation of tracer data.

Fluorinated and sulfonated hydrocarbons show great promise for use as geothermal tracers, based on a few thermal stability experiments. These tracers are detectable at very low concentrations and can be obtained in a number of species, so that a number of wells can be tested simultaneously. Field application of the tracers is necessary to evaluate the practicality of their use in field situations.

Laboratory and computer simulation studies of tracer migration through fracture networks have been used to determine processes involved in tracer transport. The transfer of tracer through fracture junctions is based on laminar viscous flow, where tracer follows streamlines. Some movement of tracer between streamlines is driven by molecular diffusion. The FRACSL code has been used to analyze data from laboratory physical models and from the East Mesa geothermal field. Simulation of tracer recovery data from East Mesa provided an estimate of hydraulic gradient and an anisotropy ratio for formation permeability.

2. NUMERICAL AND PHYSICAL MODELING OF SOLUTE TRANSPORT IN FRACTURE JUNCTIONS

John D. Miller and Laurence C. Hull
Hydrology
Idaho National Engineering Laboratory
Idaho Falls, ID

Solute (tracer) transport through the junction of multiple parallel plate fractures has been modeled by describing the movement of imaginary marker particles through the junction. The model has been integrated into the FRACSL code as part of a 2-D simulation of laminar viscous flow and solute transport in saturated fractured media. Particles entering the junction at a given lateral position in an inlet fracture are moved along streamlines to a computed lateral position in the appropriate exit fracture. Motion due to molecular diffusion is approximated for a limited class of junctions. The model includes a junction in a flow regime driven by multiple sources or sinks. A representative model is provided for this case in the absence of a unique solution. A physical model was used to verify the FRACSL algorithm for a system of fractures with simple junctions.

2.1 Introduction

The FRACSL code (Clemo and Miller, 1985) simulates groundwater flow and solute transport in a fractured geologic media under two-dimensional, isothermal, saturated conditions. The FRACSL models are implemented and solved using a continuous differential equation solver, the Advanced Continuous Simulation Language (Mitchell and Gauthier Associates, 1981). The fractured media is represented by rectangular matrix blocks with discrete fractures superimposed on their edges and diagonals. Separate matrix and fracture flows are computed, driven by a common head distribution. Solute transport is simulated by moving imaginary marker particles, each tagged with a specific amount of solute, through the matrix and fracture flow fields. Marker particle movement in the matrix due to advective, dispersive, and diffusive effects is simulated as is marker particle movement in the fractures due to advective and diffusive components. Transfers between fractures and matrix are made on the basis of computed trajectories and the geometry of the fracture system. Solute concentration is established by the distribution of the marker particles at any time in a simulation.

This discussion presents one of the suite of marker particle movement models: the transfer of a particle from one fracture into an intersecting fracture. Longitudinal and lateral velocities in the fracture, combined with random diffusive movements, establish the particle lateral position as it enters a junction. The junction may have multiple inlets and multiple exits. The transfer model establishes, for given geometry and branch flows, the routing of the individual streams. Individual particle paths are then calculated on appropriate streamlines through the junction. Tracer transfer between streamlines due to diffusive movement can be included in the calculation.

2.2 Approach

This study is limited to the laminar, streamline flow condition which exists in all fracture flow situations with the possible exception of the vicinity of an injection or production well. The study is further limited to the isothermal, saturated flow of water at fixed density and with a dissolved solute (no suspensions). The fractures are idealized as parallel-sided and with flow limited to two dimensions. The fracture junction may consist of a maximum of eight branches. Flow in the junction area is described as a number of discrete streams each originating at a fully developed region of an inlet fracture, moving through a transition, the junction itself, a second transition and terminating at a fully developed region of an exit fracture. Simulations with the SALE (Simplified Arbitrary Lagrangian-Eulerian) fluid dynamics code (Amsden et al., 1980) have shown that the Poiseuille profile is almost completely established within two channel widths from the junction, in either inlet or exit branches. Fracture apertures are a very small fraction of their length as shown, for example, by Rouleau and Gale (1984). The travel in a total

transition length equal to four apertures is therefore neglected. Therefore, the model presented in this report transfers a particle from an established lateral position at the end of an inlet fracture to a lateral position at the beginning of the appropriate exit fracture by following a streamline through the junction. In addition, solute can diffuse laterally between streamlines based on a calculated residence time in the junction.

2.3 Stream Routing

2.3.1 Continuous Sequences. Figure 2.1 shows a simple four-branch fracture junction which illustrates the approach and the format used throughout this discussion. As shown at the top of the figure, volumetric flows of six and four units enter from the right and top, respectively. Flows of seven and three units leave from the left and bottom, respectively. The sequence of inlet branches is continuous, i.e., not interrupted by an exit fracture.

The center sketch shows the actual streamlines. Streamline A is at the inlet (and exit) origin of the flow scale and, as indicated in the center figure, moves from the edge of Branch 3 to the edge of Branch 2. The other streamlines show the overall flow pattern: Branch 3 dominates, filling Branch 2 and part of Branch 1. Two basic properties are illustrated: no streamline crosses another, and streamlines from adjacent branches, e.g., B and C, are in the same direction for most of their length. Shown around the outside of the middle sketch are the flow scales: counterclockwise (CCW) from due east for the inlet flow and clockwise (CW) from due east for the exit flow.

The sketch at the bottom of the figure is a schematic of the transfer function used in the model. The vertical scale is cumulative flow running from zero at the top of the figure to the total inlet flow (or exit flow) at the bottom of the figure. The left side of the sketch is the junction inlet scale and the right side the exit scale. The inlet scale begins with the first inlet streamline starting at due east and proceeding CCW around the junction. The branches encountered in this sweep are shown on the figure; first No. 3 and then No. 4. The exit scale on the right side of the figure represents the exit streamlines in CW sequence around the junction from the first inlet streamline. Branches 2 and 1 are encountered in that order. Streamlines are indicated on this figure by the horizontal arrows labeled A through F.

Also shown in the lower sketch are the particle location extremes in each branch. Lateral particle (fractional) position, as represented in FRACSL, ranges from 0 at the left edge of vertical or diagonal fractures and the bottom of horizontal fractures to 1.0 at the opposite edge. The zero edge is shown by an arrow from a small circle and the 1.0 edge by an arrow to a line.

This approach is applied to continuous inlet sequences for fracture junctions of any number of branches up to the maximum of eight treated by FRACSL.

2.3.2 Discontinuous Sequences. A fracture junction of three branches is continuous for any reservoir condition since any two inlet branches must be adjacent. Discontinuous sequences may exist for junctions of four or more branches in reservoirs with multiple production or injection wells.

Figures 2.2 through 2.4 show different candidate routings for a discontinuous four branch sequence. Note that Branch 4 interrupts the sequence of inlet branches, 3 and 1. Each of the routings satisfies continuity, i.e., each provides six flow units in from the right, four in from the left, six out the top, and four out the bottom. In addition, none have crossing streamlines.

Figure 2.2 shows the maximum right-to-top flow of six units. The streamline distribution is shown in the center sketch of Figure 2.2. While no streamlines cross in this routing scheme, adjacent streamlines A and C travel in opposite directions. The alignment of branches to achieve this flow distribution is shown in the bottom sketch of Figure 2.2.

Figure 2.3 shows a six unit right-to-top flow. The flow configuration is acceptable; streamlines from adjacent branches are in the same direction for the majority of their length. The essential features of the arrangement in this figure are the following: the exit scale is started with the first exit fracture (No. 2) CW of the first inlet fracture. This is the convention adopted for the continuous case: the inlet scale proceeds CCW and the exit scale proceeds CW from the same point on the circumference of the junction. The next exit fracture (No. 4) spans the break between inlet fractures (3 and 1). The exit scale is completed by the initial exit fracture which, therefore, spans the other break between the two inlet fractures. It is this relative positioning, with each exit fracture spanning the

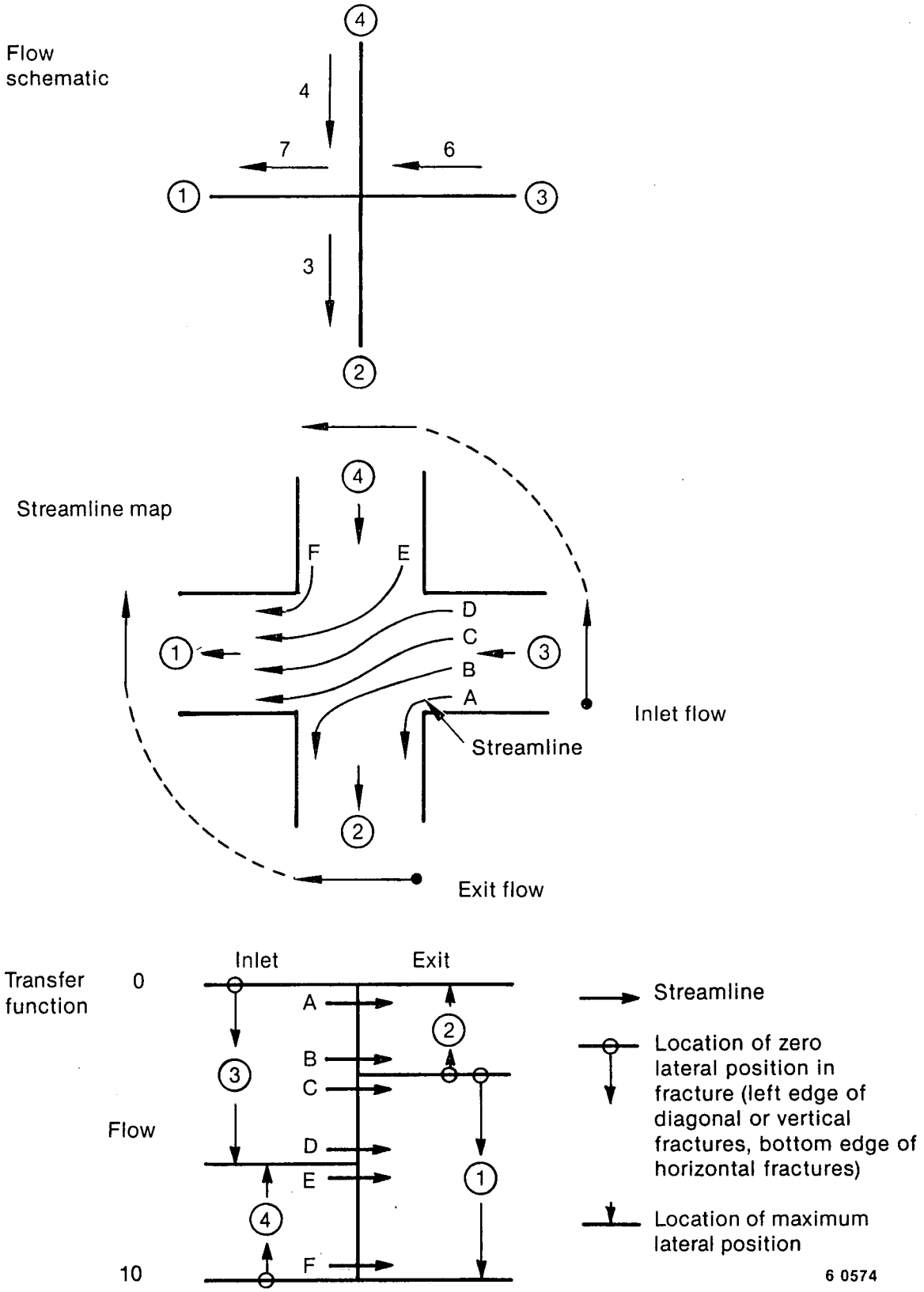

Figure 2.1 Simple four-branch fracture junction.

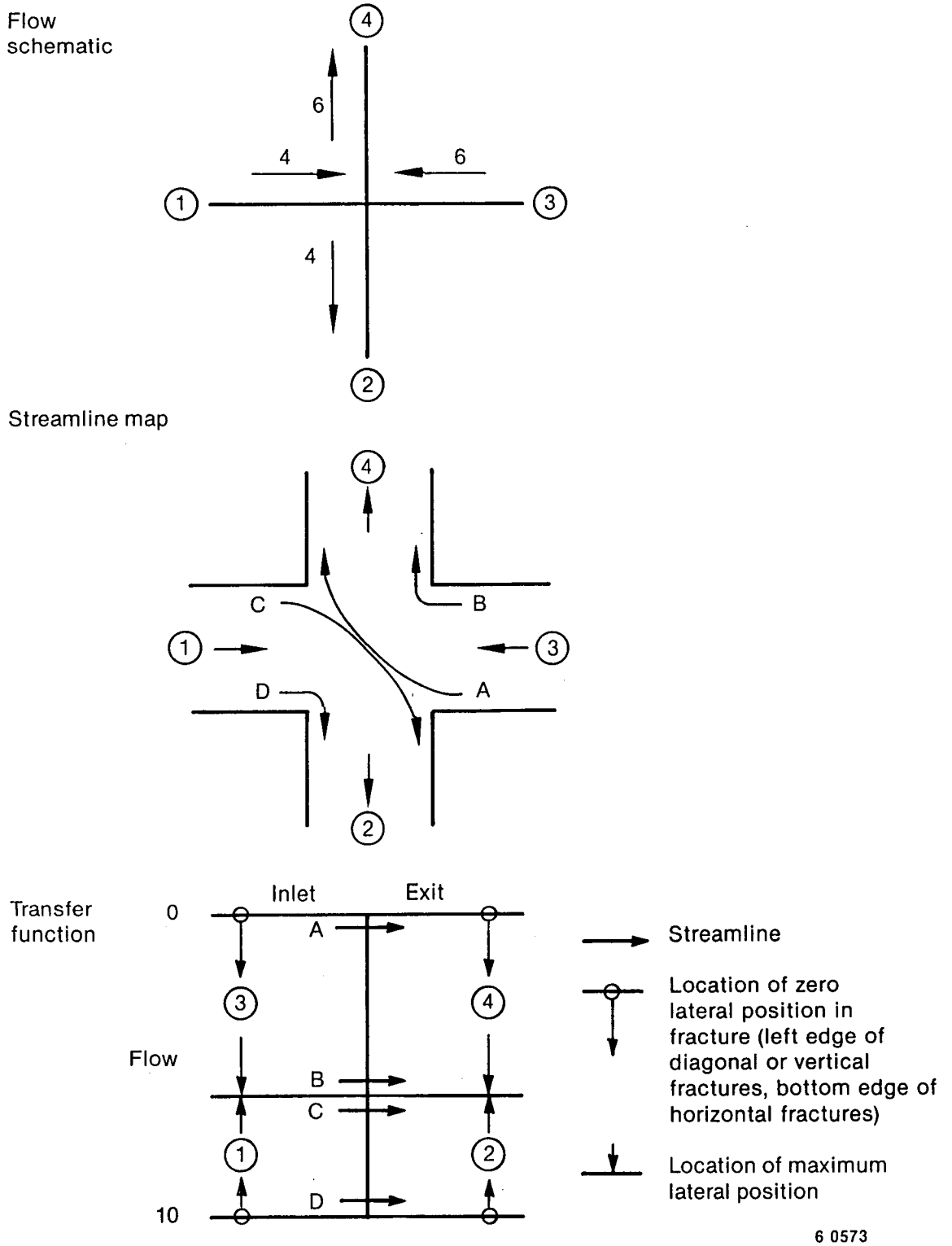

Figure 2.2 Four-branch discontinuous fracture junction, six unit right-to-top flow.

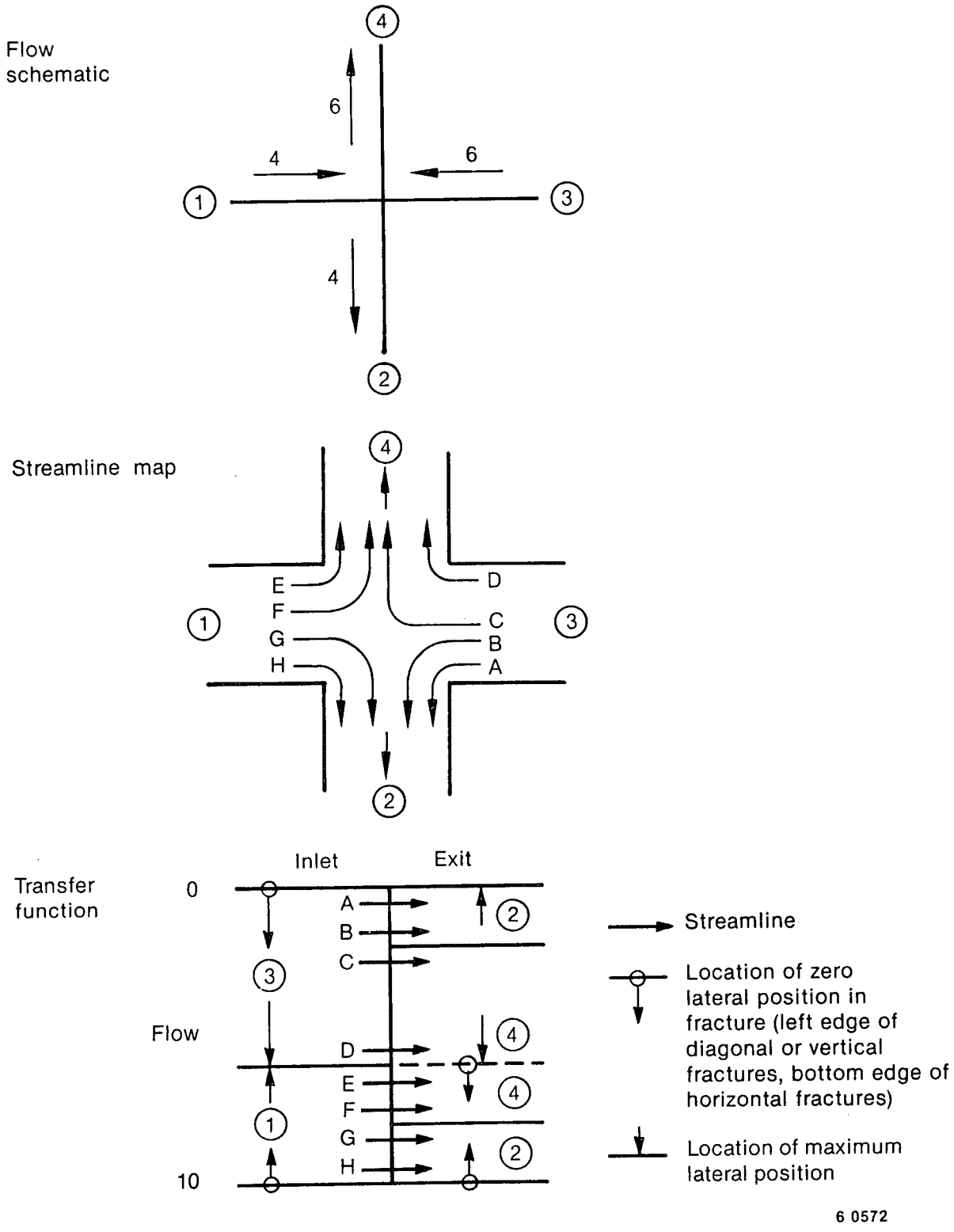

Figure 2.3 Four-branch discontinuous fracture junction, six unit right-to-top flow.

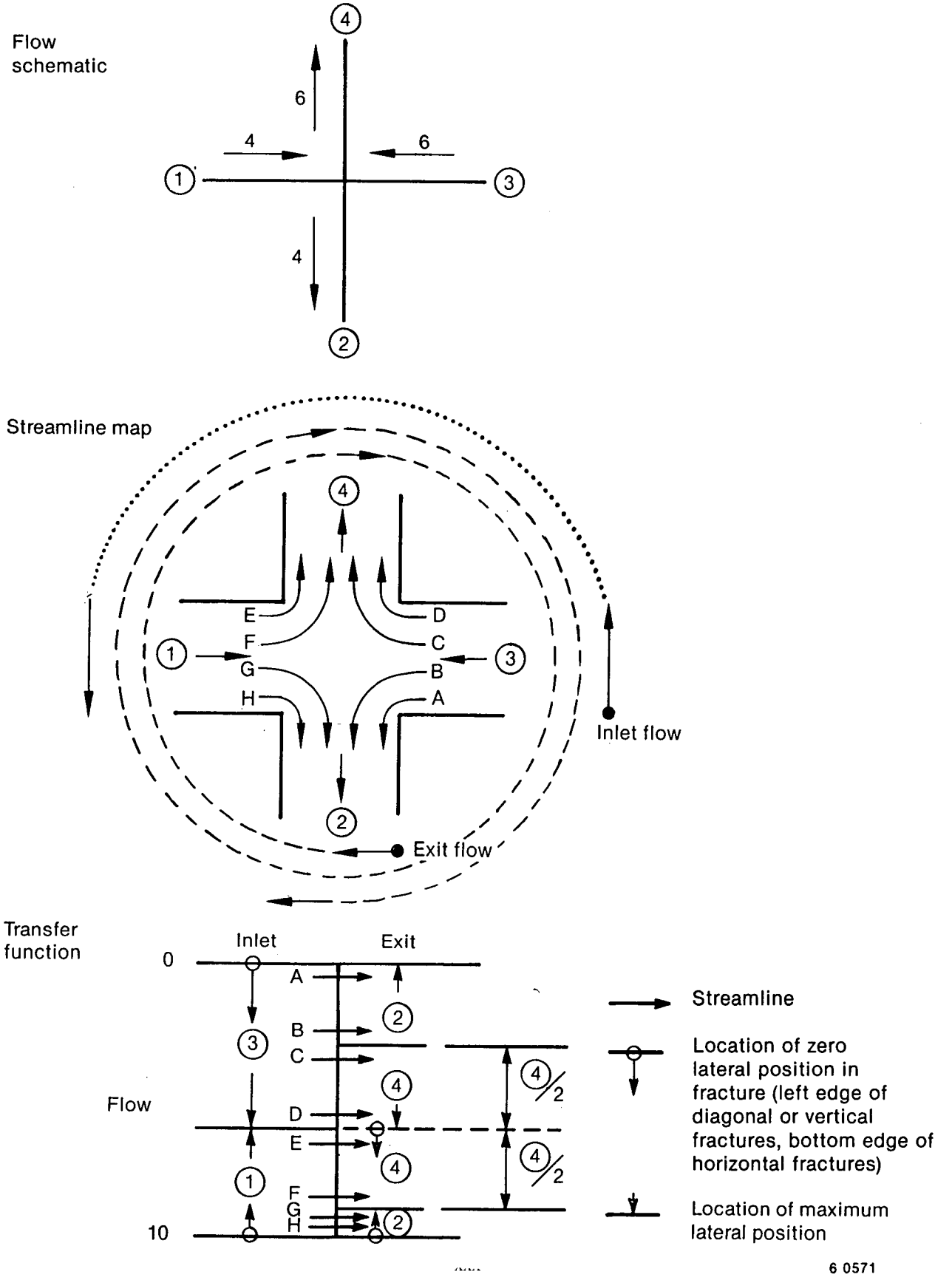

Figure 2.4 Four-branch discontinuous fracture junction, six unit right-to-top flow.

break between inlet fractures, which provides each exit some of the inlet flow from each neighbor and prevents opposing streamlines.

Figure 2.4 shows a six unit right-to-top flow. An acceptable streamline pattern results, as shown in the middle sketch. The circular layouts of the exit scale on this diagram incorporate two complete revolutions of the figure plus a small additional amount. Note that the exit flow in Branch 4 between Streamlines C and D is placed on the cumulative flow scale before the first (CW) part of the fracture between Streamlines E and F.

Figure 2.3 corresponds to centering the first exit stream (CW of first inlet stream) on its neighboring inlets. Figure 2.4 corresponds to centering the second exit stream on its neighboring inlets. In any case, each exit fracture must span the break between physically separated inlets. The existence and the identity of a unique solution has been studied using simple analytic techniques without success. Ultimate resolution requires further analytic or physical model studies, or the use of a basic fluid dynamics code.

The strategy used in the program centers the initial exit group on the beginning—end of the exit flow scale. The entire sequence is shifted as necessary to assure that each group of exit fractures spans a break between inlet fracture groups.

Studies on a discontinuous junction of five branches have shown that the strategy may be applied by grouping adjacent inlet (or exit) branches. Tests on a larger number of branches have not been conducted. The selected strategy should, however, be equally valid.

2.4 Stream Velocity Profiles

Individual streamlines are traced through a fracture junction by matching the cumulative flow from the origin of the exit flow scale to the same cumulative flow (from the same origin) on the inlet flow scale. For example, in Figure 2.1 streamline E enters the junction approximately 6.5 units from the origin of the inlet scale and leaves the junction 6.5 units from the origin of the exit scale. The position of a streamline in a particular fracture and the flow between that streamline and the edge of that fracture are related by the properties of the Poiseuille velocity profile.

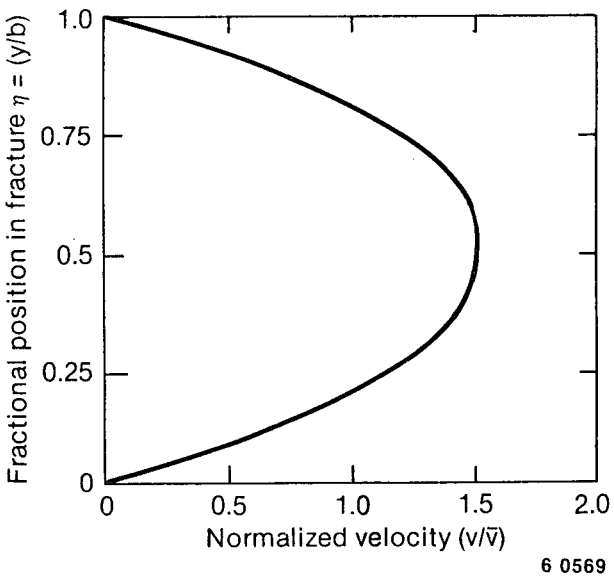

Figure 2.5 Fracture velocity as a function of fractional location in fracture.

The Poiseuille profile for laminar viscous flow in a channel of unit depth and width b gives the velocity at distance y from the edge of the fracture as:

$$v = 6\bar{v}\,[y/b - (y/b)^2] \qquad (2.1)$$

where $\bar{v}$ is the average velocity across the channel. This profile is continuous over the succession of streams comprising the combined flow. With η as the fractional distance from the edge of a channel (Figure 2.5), the flow between a streamline at fractional position η_1 and the edge of the fracture is found as

$$Q_1 = \int_0^{\eta_1} vbd\eta \quad . \qquad (2.2)$$

Substituting for v from Equation 2.1 and integrating:

$$Q_1 = 6\bar{v}b \int_0^{\eta_1} (\eta - \eta^2)\, d\eta = 6\bar{v}b \left(\frac{\eta_1^2}{2} - \frac{\eta_1^3}{3}\right) \qquad (2.3)$$

After choosing the correct root the cubic equation above is solved for η_1 as:

$$\eta_1 = \cos\left[\frac{1}{3}\cos^{-1}\left(1 - \frac{2Q_1}{\bar{v}b}\right) + \frac{4\pi}{3}\right] + \frac{1}{2} \quad . \qquad (2.4)$$

These relationships are used to trace streamlines through the fracture junction in a two-step

procedure. In the first step, the steam routing described in the previous section is determined and the cumulative flow rates at the edges of each of the inlet and exit fractures are determined as illustrated in the center sketch in Figure 2.1. These flow rates define the transfer structure which is maintained until the system flow rates are changed.

In the second step, streamlines are determined for each of the individual particles. A cumulative inlet flow rate, QABS, is determined for an entering particle as the sum of its flow increment from the fracture edge (Equation 2.3) plus the cumulative flow at that edge. For streamline E in Figure 2.1, this is equal to 0.5 + 6.0. Moving to the exit side, the streamline is located in the appropriate exit facture (1) and the flow from the edge of that fracture found (3.5 = 6.5 - 3.0). Equation 2.4 is then used to determine the position in that fracture. Lateral motion due to diffusion, for certain junctions, is determined by a preliminary step described in the following section.

2.5 Molecular Diffusion and Mixing

Diffusive movement results in lateral transfer of tracer between streamlines and some mixing between streams in a fracture junction. The limiting case of complete homogenization of tracer will only occur at very low flow rates. Mixing in junctions is implemented by modifying the position of the solute particle on the inlet discharge scale before moving it across the junction.

Complete random mixing is provided for comparison of results to other transport codes currently available which use the complete mixing approach. This option is implemented by randomizing the position of the particle on the cumulative inflow scale. The particle can then exit the junction by any exit fracture, with a probability determined by the discharge through the exit fractures.

Diffusive motion is based on a residence time in the fracture junction. Residence time is approximated as the distance a particle travels across the junction divided by the velocity of the particle as it enters the junction. Distance is assumed to be linearly related to the position of the particle on the cumulative inlet scale ranging from 0 at the two ends of the cumulative inlet scale to the junction diagonal at the center. Referring to Figure 2.1, particles in streamlines A and F travel very short distances, while particles in streamlines C and D travel much further. This configuration is strictly valid only for a junction of four branches where the two inlet and two exit fractures all have equal flows.

Velocity is based on the particle's inlet velocity. This does not account for acceleration in the junction, which would require an iterative technique. Velocity is calculated from Equation (2.1). The transverse movement of a particle (Δy) due to diffusion is calculated from:

$$\Delta y = (2D_m x/v)^{1/2} \text{ ANORM} \quad . \qquad (2.5)$$

This Δy must be transformed from a linear distance scale to a discharge scale before modifying the inlet position of a particle. This is done using the derivative of the velocity profile equation,

$$\Delta Q = 6v[y/b - (y/b)^2] \Delta y \quad . \qquad (2.6)$$

The ΔQ calculated from Equation (2.6) is used to modify the particle position on the inlet discharge scale. Particles displaced beyond the range of the cumulative inlet scale are reflected back into the range by the amount they fell outside the range. The outlet position is then calculated by the junction transfer function in the usual manner.

2.6 Laboratory Testing and FRACSL Simulation

2.6.1 Laboratory Physical Model. The laboratory physical model (Figure 2.6) is built of plexiglas to allow both visual and electronic monitoring of tracer movement using dye and salts added to solution. Two sets of continuous, orthogonal fractures were cut, using a milling machine, into a 172 cm by 58 cm sheet of plexiglas. The tops of the fractures were then sealed using a second, thin sheet of plexiglas. Fracture aperture is 0.32 cm and height 1.90 cm with a tolerance of ± 0.002 cm. Fracture spacing is a uniform 10.2 cm. All fractures are continuous and meet the model boundaries at 45 degrees. Nineteen electrodes are embedded in the fracture walls to quantify tracer movement through the model. Electrodes are scanned periodically using a computerized data acquisition system to record fluid conductance. The probes are multiplexed to avoid crosstalk.

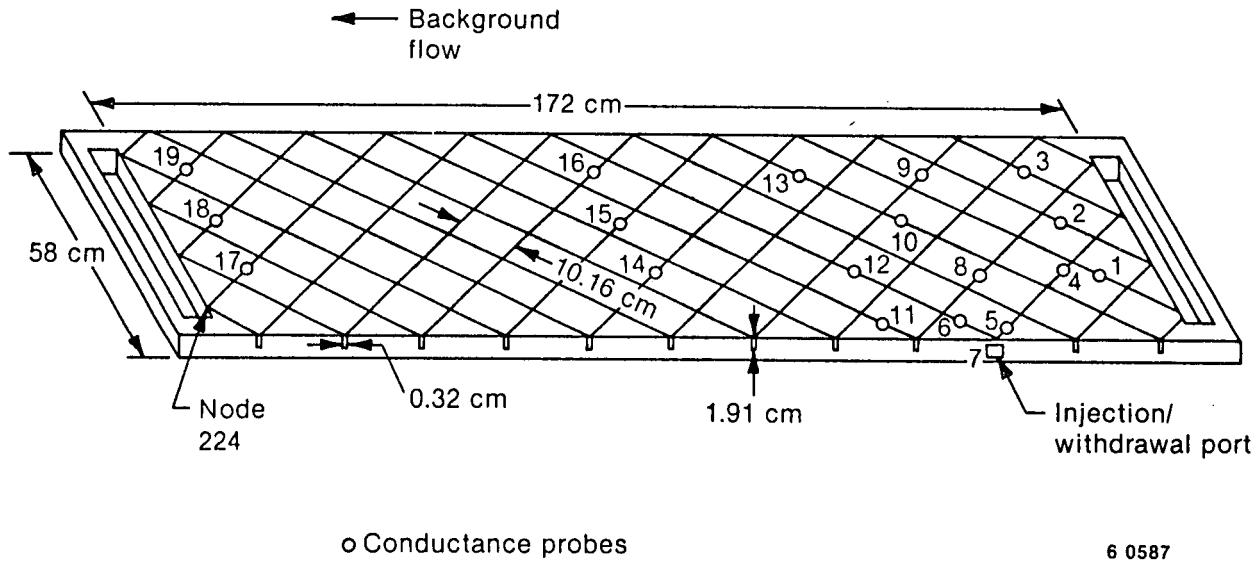

Figure 2.6 Laboratory physical model used for tracer testing.

Density effects are a major concern for tracer selection. Using the same salt at two different concentrations for native fluid and tracer (0.25E-04 and 1.0E-04 molar) is sufficient to produce density effects. In preliminary laboratory tests, the higher concentration injected fluid flowed under the native fluid in the fractures instead of displacing it completely. This had significant effects on the spread of the tracer in the model. To avoid density effects, two different salts with different molecular weights are used. When equal masses of the two salts are used to make up the native and tracer solutions, the solutions have equal densities but contrasting conductances.

2.6.2 Laboratory Testing. The test used to study the effects of diffusion on tracer movement in fracture systems consisted of two phases. During the first phase, tracer was injected into the reservoir through a port in the side of the model while a background flow was passing through the model. The second phase consisted of drift in the reservoir sweeping out the injected tracer plume. A flow field of 5.26 cm^3/min was established in the fracture network model using $0.84*10^{-4}$ molar $CsCl_4$. A $2.27*10^{-4}$ molar KCl tracer solution was injected at a rate of 3.36 cm^3/min for 27.5 min into a port on the side of the model (Figure 2.6). Total outflow from the model was constrained to be 5.26 cm^3/min, so discharge from the model was constant whether or not injection was occurring.

2.6.3 FRACSL Simulations. FRACSL treats transport on a mechanistic level. Tracer dispersion is based on development of a velocity profile between the walls of the fracture, and diffusion across streamlines. Consequently, there are no empirical dispersion coefficients required by the model, only a diffusion coefficient which can be readily obtained from the literature. For the diffusion of KCl and CsCl, the diffusion coefficient, D_m, is 1.09×10^{-3} cm^2/min at 20°C (Miller, 1982).

Figures 2.7 through 2.11 give examples of fits between the laboratory data and the FRACSL simulation using $D_m = 1.09 \times 10^{-3}$ cm^2/min. Electrode locations are shown in Figure 2.6. Electrode 6 is immediately adjacent to the injection port. Tracer breakthrough at this electrode represents transport through a single fracture (Figure 2.7). Electrodes 11, 14, and 17 (Figures 2.8, 2.9, and 2.10) are at increasing distances from the injection port. By the time the tracer has reached Electrode 17, it has traveled through 18 fractures and 10 fracture junctions. The simulated peak tends to spread out more than the measured peak with increasing distance from the injection port. This results in lower peak heights and a longer tail for the simulated results. The total mass of tracer, however, is matched fairly well.

No tracer can reach Electrode 18 by advection alone, i.e., following streamlines. The only means for tracer to reach this electrode is by diffusing across streamlines both within fractures and at fracture junctions. Figure 2.11 shows that in both the simulation and laboratory, tracer does reach

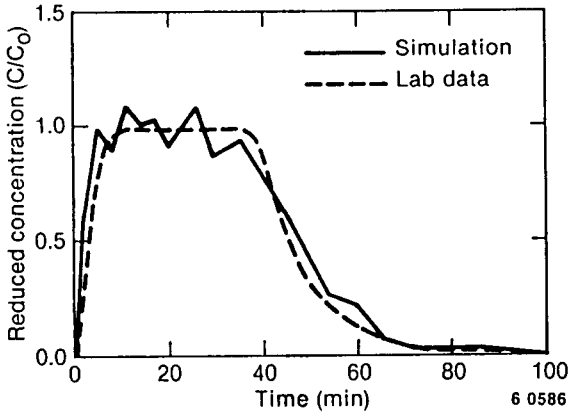

Figure 2.7 Comparison of tracer concentration data from the laboratory physical model with FRACSL simulated concentrations for Electrode 6.

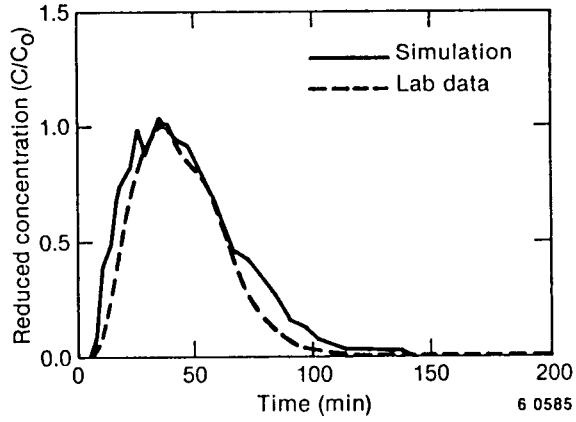

Figure 2.8 Comparison of tracer concentration data from the laboratory physical model with FRACSL simulated concentrations for Electrode 11.

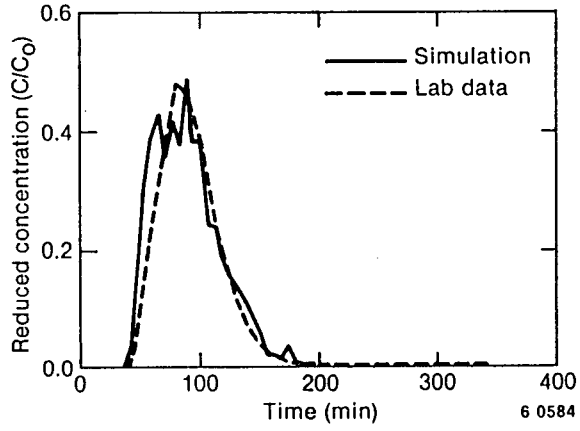

Figure 2.9 Comparison of tracer concentration data from the laboratory physical model with FRACSL simulated concentrations for Electrode 14.

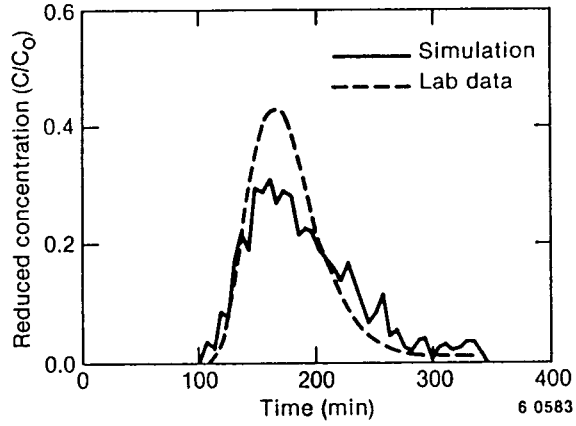

Figure 2.10 Comparison of tracer concentration data from the laboratory physical model with FRACSL simulated concentrations for Electrode 17.

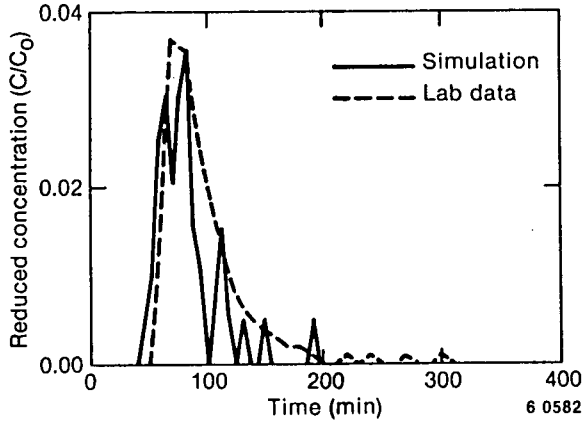

Figure 2.11 Comparison of tracer concentration data from the laboratory physical model with FRACSL simulated concentrations for Electrode 18.

Electrode 18. Because this electrode is very near the edge of the tracer plume, the sparse number of particles in the simulation result in a very "noisy" simulated breakthrough curve.

To test the sensitivity of the simulations to changes in the diffusion coefficient, simulations of the physical model test were made with the FRACSL code using diffusion coefficients ranging from 0.55 x 10^{-3} to 2.2 x 10^{-3} cm^2/min. To quantify how well the simulations matched the laboratory data, a χ^2 was calculated using the integrated area under the tracer breakthrough curves. Thus, the goodness-of-fit criteria is based on the mass of tracer passing an electrode. The results are shown in Table 2.1. There is a minimum in the χ^2 values at a diffusion coefficient of 1.6 x 10^{-3} cm^2/min.

Simulations were also made for two other cases, following streamlines through the model, and for homogenization at fracture junctions. The simulation of streamlines was achieved by setting the diffusion coefficient to zero. Thus, there was no mixing of tracer either within fractures or at fracture junctions. The second end-member case involved complete mixing at junctions. Tracer entering a junction could leave by any exit fracture with a probability dependent on discharge through the exits. In addition to assuming complete mixing at junctions, it was also assumed that all tracer traveled at the average fluid velocity within the fractures. Simulations based on both these assumptions resulted in much poorer fits to the laboratory data (Table 2.1).

The assumptions used in simulating tracer migration affect the outcome. The best fit between the laboratory data and computer simulations included transverse mixing by diffusion, both in fractures and in fracture junctions. The best fit to the data was obtained using a diffusion coefficient about 50% higher than that calculated from ion mobility data. This probably indicates that the laboratory model boundary conditions are not as ideal as those incorporated into the computer simulation. Based on the general agreement between the laboratory data and the computer simulation, it is concluded that transfer of tracer across streamlines plays a significant role in dispersion of solutes in fracture systems.

Table 2.1. Chi square statistics for measuring fit of computer simulations to laboratory data

Diffusion Coefficient (*10^3 cm^2/min)	χ^2 Electrodes 5, 6, 11, 12 14, 15, 17, 18
0.0 (streamlines)	15.5
0.55	8.6
1.09	6.0
1.30	7.6
1.60	3.6
1.90	5.9
2.20	7.6
Complete mixing	80.3

$$\chi^2 = \frac{(\text{lab - simulation})^2}{\text{lab}}$$

2.7 Discussion

Diffusion between streamlines can be used to explain the dispersion observed in the laboratory physical model. This means that even at relatively high flow rates, a streamline approach to transport in fractures will underestimate dispersion. While residence time in fracture junctions is commonly considered to be negligible, there is a distribution of residence times. Flow entering from the center of a fracture moves very rapidly through a junction, and there is little time for diffusion. Flow along the fracture wall, however, will be moving very slowly as it enters a junction. Depending on the arrangement of fractures and the magnitude of the flow from each, this slow moving fluid may or may not be accelerated through the junction. As a result of this distribution of residence times, some tracer solution may have sufficient time to diffuse laterally across streamlines that leave the junction by different fractures.

In addition to lateral diffusion in fracture junctions, lateral diffusion occurs within fractures. Because of longer residence times in fractures than in junctions, the lateral mixing within fractures may be much more important. For transverse diffusion to homogenize tracer within a fracture, the dimensionless diffusion time must be greater than about 0.5 (Crank, 1975),

$$D_m t/b^2 > 0.5 \quad . \tag{2.7}$$

This homogenization must take place in the time it takes tracer to travel between fracture junctions at the peak rate along the center of the fracture,

$$\bar{v}t/x > 0.67 \quad . \tag{2.8}$$

Solving the Equations (2.7) and (2.8) for time, and requiring the fracture residence time to be greater than the diffusion time, gives a Peclet number for fractures,

$$D_m \, x/\bar{v}b^2 > 0.75 \quad . \tag{2.9}$$

For a diffusion coefficient of 10^{-3} cm^2/min, a fracture aperture of 0.1 cm, and a fracture spacing of 1 m, homogenization will occur at any average velocity less than about 200 m/day.

At junctions, however, a streamline approach will be a reasonable approximation down to much lower velocities, and complete mixing will not occur until very low velocities. The lower limits for streamlines and upper limits for complete mixing at junctions can be calculated by considering how long it takes diffusion to move tracer between streamlines. For purposes of the calculation, assume two equal aperture fractures meeting at 90 degrees with a hydraulic gradient bisecting the intersection angle. This will cause all the streamlines from each entrance fracture to leave by a single exit fracture with no crossover of flow. The residence time in the fracture junction is the distance the fluid must move divided by the rate at which it is moving:

$$t = (b/\sqrt{2})/(1.5\bar{v}) \quad . \tag{2.10}$$

The dimensionless diffusion time it takes for 5% of the tracer to diffuse across the central boundary of the fracture junction is about 0.005. For complete mixing, the dimensionless diffusion time needs to be greater than 0.5. Figure 2.12 shows a plot of aperture versus velocity, and the limits for pure advection and complete mixing at junctions.

2.8 Conclusions

A junction transfer model has been developed, programmed as an addition to the FRACSL code, and checked out on a sample reservoir model. The algorithm determines the exit fracture and lateral position in that fracture for a marker particle entering the junction in a specified fracture and at a specified position within that fracture. This algorithm completes the suite of marker particle algorithms used to simulate flow and solute transport in the FRACSL code. Laboratory tests found generally good agreement between measured and predicted dispersion for the laboratory model. Somewhat greater spreading in the laboratory model is probably due to more complex boundary conditions in the laboratory model than are being simulated. This generally good agreement is interpreted to mean that mixing by diffusion in fracture junctions is the mechanism responsible for transverse dispersion in fracture networks.

Based on this finding, calculations can be made to show under what conditions certain common simplifying assumptions can be made. For geothermal reservoir applications, complete mixing at junctions is probably not justified. Homogenization in fractures in geothermal reservoirs will depend on fracture system geometry and local flow rates. To permit a completely general approach to simulation of flow and transport in fracture systems, the FRACSL code includes no assumptions about mixing at junctions or homogenization within fractures. The mechanistic approach used in FRACSL permits its application to any laminar flow situation.

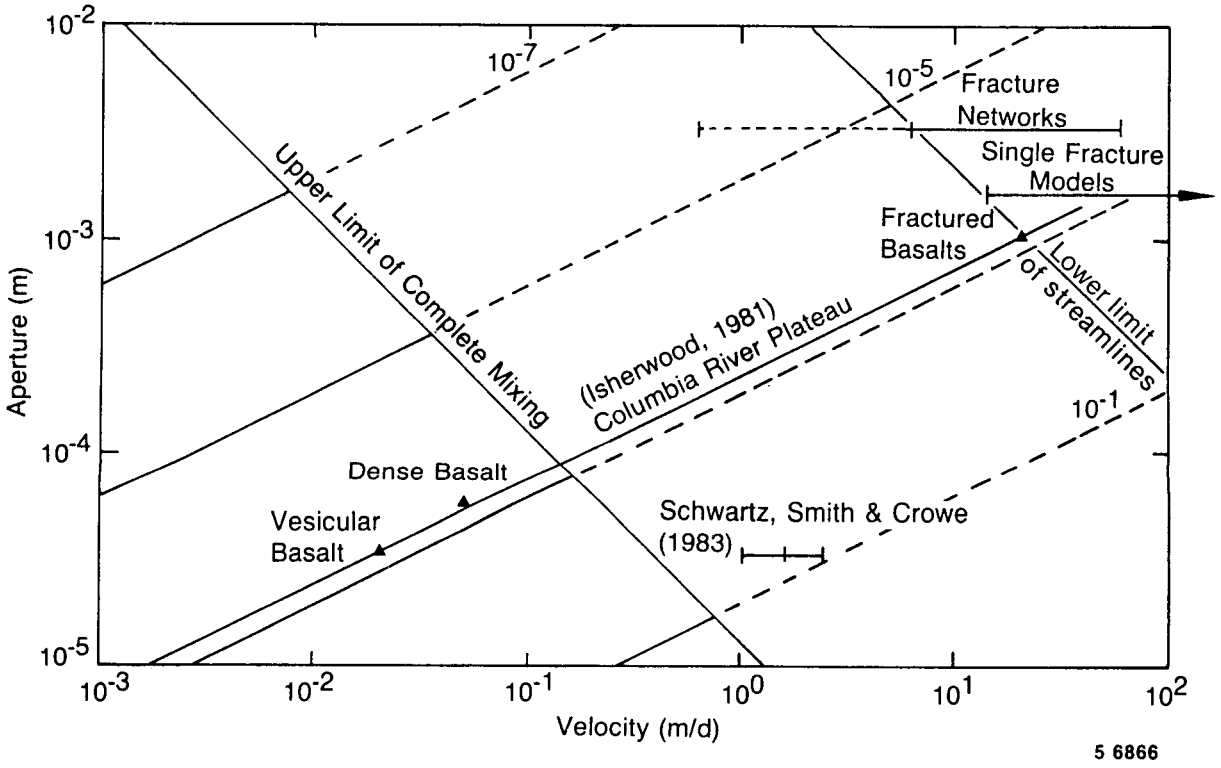

Figure 2.12 Maximum velocities in fractures of various apertures that permit sufficient residence time for mixing to occur due to molecular diffusion. Diagonal lines from lower left to upper right represent lines of constant hydraulic gradient.

2.9 References

A. A. Amsden, H. M. Ruppel, C. W. Hirt, *SALE: A Simplified ALE Computer Program for Fluid Flow at All Speeds*, LA-8095, Los Alamos National Laboratory, 1980.

T. M. Clemo and J. D. Miller, *Fractured Media—Advanced Continuous Simulation Language (FRACSL) User's Guide*, EG&G Idaho Internal Report, Idaho National Engineering Laboratory, 1985.

J. Crank, *The Mathematics of Diffusion*, London: Oxford University Press, 1975.

D. G. Miller, *Estimation of Tracer Diffusion Coefficients of Ions in Aqueous Solution*, UCRL-53319, Lawrence Livermore National Laboratory, 1982.

Mitchell and Gauthier Associates, *Advanced Continuous Simulation Language (ACSL) User's Guide and Reference Manual*, Mitchell and Gauthier Assoc., P.O. Box 685, Concord, MA, 1981.

A. Rouleau and J. E. Gale, "Statistical Characterization and Numerical Simulation of a Fracture System for Hydrogeological Purposes," *International Groundwater Symposium on Groundwater Resources Utilization and Contaminant Hydrogeology, Montreal, Canada, 1984*, pp. 188-196.

3. FRACSL CODE STATUS AND VERIFICATION STUDIES

Tom M. Clemo and Laurence C. Hull
Hydrology
Idaho National Engineering Laboratory
Idaho Falls, ID

3.1 Introduction

The FRACSL reservoir simulation code was created to fill a need for analysis of solute transport in dual-permeability reservoirs. In reservoir simulations, dual-permeability refers to the existence of high permeability discrete fractures in conjunction with a lower permeability continuum, which may be porous material or a finer scale fracture network. Few existing codes address both regimes and none adequately combine this with solute transport modeling.

FRACSL solves the pressure and flow distribution using lumped parameter modeling techniques. The matrix material is defined using a grid structure with nodes at the intersection of grid lines. The discrete fractures exist as connections of adjacent nodes. Pressures are calculated for the nodes, and the pressure distribution is used to drive solute particle movement. Solute particles can exist in both the fractures and the matrix. Discrete solute particles are not only driven by the pressure and flow distribution, but are also affected by dispersion and diffusion. These are modeled as random processes using Monte Carlo routines.

The FRACSL code uses a direct simulation approach to solute transport by the use of discrete representative particles. These particles are moved about the grid under the influence of the pressure and flow calculated to exist in the reservoir. Direct simulation was chosen over a continuous distribution because of the complex nature of a discrete fracture representation and the concern over numerical dispersion problems inherent in numerical solutions to the advection-dispersion equation.

During FY-83 and FY-84, the basic components of the FRACSL code were created. The major components of the code were:

- Definition of the reservoir and input routines to support it,
- Calculation of the pressure distribution,
- Movement of the solute particles in both fractures and the matrix,
- Transfer of particles from one type of element to another,
- Simulation of tracer injection and recovery, and
- Plotting routines based on the INEL ISDMS plotting packages.

During FY-85 FRACSL was improved in three areas. In the first area, improvements and corrections to the basic components were driven by experience gained from using the code in modeling applications. Secondly, new capabilities were added to the code, which did not exist in the FY-84 code, to meet requirements of modeling applications. The final area of improvement was in the ease of use of the code. Experience has shown that the time spent on simplifying the use of FRACSL has been quickly recovered in subsequent modeling efforts.

3.2 Code Elements

This section describes the code as it existed at the end of FY-84. Development during FY-85 is discussed in Section 3.3.

3.2.1 Reservoir Nodalization and Physical Description. FRACSL simulates a two-dimensional reservoir of unit thickness using Cartesian coordinates and a rectangular pattern of nodalization. The nodes are located at the intersection of rows and columns. Figure 3.1 presents an example of a FRACSL model. Shown are the rows and columns with nodes at the intersections. The

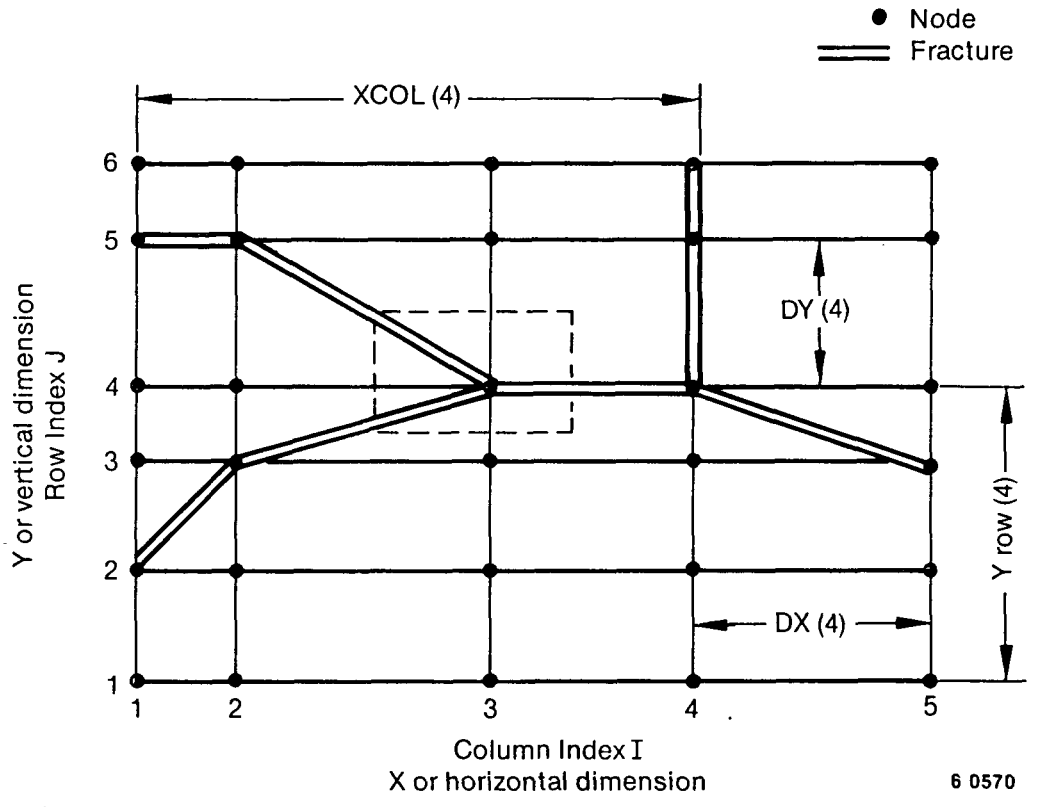

Figure 3.1 Example FRACSL model.

dotted line surrounding the central node is an example of the area to be associated with a node for fluid accounting purposes. The pressure at the node is the average pressure of the nodal volume. The double lines are major fractures connecting nodes. Fractures are restricted to connections between adjacent nodes, and only one diagonal fracture may occur in a cell.

A fracture is defined by specifying the two nodes it connects and is only valid if it connects adjacent nodes. The fracture segment length and angle are calculated by the code. The fracture aperture is either input or calculated from the overall multisegment fracture length. If a fracture has a porosity different from one, the porosity may be specified. Fracture conductivity is calculated from the cube of the aperture (Romm, 1966).

The rectangular blocks defined by the rows and columns are called matrix cells. These cells represent the fine fracture network and the rock itself. Matrix properties are homogenous within a cell, but can be different for each cell. The properties are indexed by material number. The matrix properties currently used are:

- Longitudinal dispersivity
- Transverse dispersivity
- Conductivity in the x direction
- Conductivity in the y direction
- Specific storage
- Porosity.

3.2.2 Flow Calculation. The FRACSL hydraulics model is based on the conservation of mass. Equation (3.1) is the conservation of mass equation for a two-dimensional system,

$$\frac{\partial(\rho V v_x)}{\partial x} + \frac{\partial(\rho V v_y)}{\partial y} = \frac{dM}{dt} + Q \quad . \qquad (3.1)$$

The head change of the node for an increase of one unit of mass is the inverse of the product of the volume of the node and its specific storage. The head response is given by:

$$\frac{dM}{dt} = \frac{\rho V}{S} \cdot \frac{d\phi}{dt} \quad . \qquad (3.2)$$

The nodal volume is computed as the sum of the volumes of the matrix and fractures in the four cell

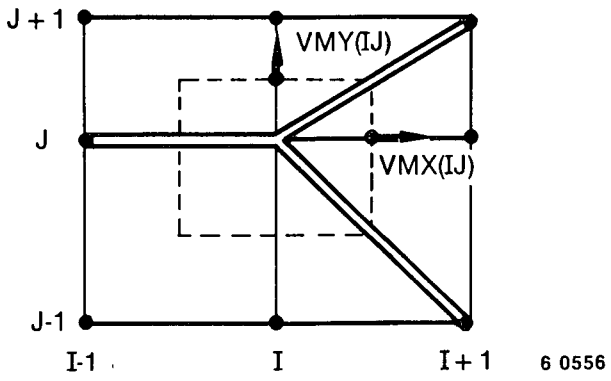

Figure 3.2 Example nodal volume.

quadrants about the node. Figure 3.2 presents the nodal volume, within the dashed lines, for an internal node. The flow across the edge of a nodal volume is determined from the head difference between the adjacent nodes. The head variation is assumed to be linear between nodes and constant along the length of the edge. Fluid velocity across the edge is found from the Darcy equation:

$$v_x = k_x \frac{\partial \phi}{\partial x} \text{ and } v_y = k_y \frac{\partial \phi}{\partial y} \quad . \tag{3.3}$$

Flow through fractures can either be laminar or turbulent. For laminar flow:

$$v = \frac{\rho g}{12\mu} b^2 \frac{d\phi}{dx} \quad . \tag{3.4}$$

For turbulent flow the flow equation is:

$$v = \left(\frac{2bg}{f_r} \frac{d\phi}{dx}\right)^{1/2} . \tag{3.5}$$

The flow regime is controlled by the Reynolds number (Re). If Re is greater than 3000, turbulence is assumed, otherwise the flow is laminar. Use of the laminar flow equations may be forced at the option of the modeler.

3.2.3 Head Calculation Control. Either time invariant or transient flow conditions can be simulated. Time invariance occurs under two circumstances; when the fluid leaving the reservoir equals the fluid entering the reservoir, or when all the heads are changing at the same rate. For the latter case, the flow solution is time invariant only for the purposes of tracer movement. An aquifer limited in areal extent or simulation of a small portion of a well developed drawdown cone are examples of the latter scenario. An iterative technique is used to solve for time invariant systems. Solute transport is then calculated using a fixed velocity distribution with the assumption that the solute does not affect the hydraulics.

The transient capability uses standard integration techniques to simulate changing flow conditions. In this case, for every time increment the hydraulic calculation is stopped, and the particle transport algorithm is executed for the time assuming a constant flow situation. The time increment, DT, is user supplied and must be chosen such that incremental changes in the head profile are small.

Further control of the dynamic flow calculation is given by the choice of integration algorithm and the maximum and minimum allowable time steps. Variable order and variable time step algorithms are most efficient for FRACSL and incorporate error control. The choices are Gear or Adams-Moulton. Gear is superior in systems where the time constants of the states (nodes) vary by more than three or four orders of magnitude. This should not be the case for most FRACSL runs and, therefore, Adams-Moulton is expected to be more appropriate.

3.3 Transport Calculation

3.3.1 Marker Particle Approach. There are two common approaches to solving solute transport problems. The traditional approach solves the advection-dispersion equation for the concentration in discrete nodal volumes. The other approach uses a discrete representation of the solute (Ahlstrom et al., 1977; Prickett et al., 1981). In this approach, the macroscopic behavior is inferred from a population of individual particles. The discrete solute approach is preferred over the classical approach in fractures, because of improved numerics and drastically reduced computer core requirements since the fractures need not be nodalized.

The FRACSL solute transport simulation uses discrete "marker particles." These particles simulate the microscopic behavior of the solute by treating diffusion and dispersion as random processes. The processes are assumed to be zero mean Gaussian and are superimposed on the deterministic advective movement. The results of a simulation are used to study the macroscopic behavior of solute transport. The macroscopic behavior is the aggregate of the microscopic behavior of each of

the individual particles. To be meaningful, the macroscopic result must be determined from a sufficient number of particle results. Sufficiency is a qualitative term and varies with application. As a general guideline, the variance of a result decreases as the square root of the number of particles used increases.

3.3.2 Particle Movement in Matrix. Movement of solute particles in the matrix requires that a head gradient be determined at the particle. Laminar, Darcy flow is assumed in the matrix. During laminar flow, the fluid velocity is proportional to the head gradient.

To obtain the local head gradient, the head at the node nearest the particle is used in conjunction with the head at the eight nodes adjacent to that node. These values allow a map to be defined which is a second order function of both the x and y particle position. From the head map, a particle velocity and acceleration can be determined. The particle movement is an Euler integration of the velocity and acceleration. The acceleration is not constant with respect to particle position. Particles are moved for a limited time with the assumption of constant acceleration. The errors inherent in this approximation are limited through the use of an error criterion.

Superimposed on the advective laminar flow movement is a simulation of fluid dispersion and diffusion. Dispersion is modeled as a random walk process with components perpendicular and parallel to the advective movement. The process is simulated as zero mean Gaussian with a variance proportional to the advective movement. Diffusion is modeled as a zero mean Gaussian process with a variance proportional the time step size.

The routine for moving particles in the matrix is composed of two elements. The first element is determination of the head gradient and curvature. The second is moving the particle within the area of validity for the head calculations and under the influence of dispersion and diffusion. Fractures complicate both the head calculation and the movement routine.

3.3.3 Effects of Fractures on Matrix Movement. The solid lines in Figure 3.3 represent all the possible fracture locations which may affect the movement of a particle in the matrix. Not all of these fractures may exist concurrently. In particular, only one diagonal fracture may exist in a matrix cell.

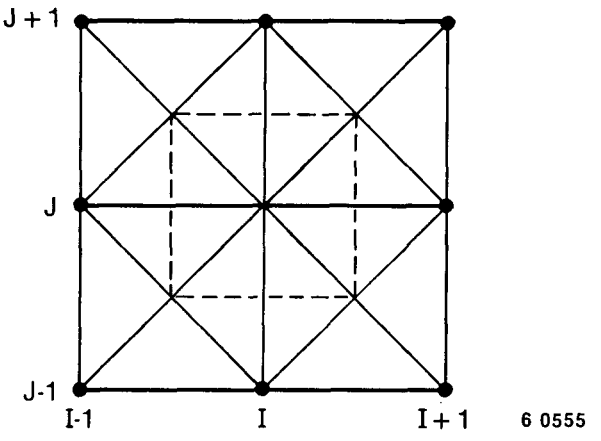

Figure 3.3 Fractures affecting particle movement in the matrix.

There are three primary features of fractures which may affect a particle's movement:

1. Head varies linearly along a fracture.

2. The first derivative of head need not be continuous across a fracture. Therefore, the head information of a node does not affect a particle if a fracture exists between the node and the particle.

3. A flow component due to local storage of fluid exists near a fracture. This represents fluid which exits the fracture and is stored within the nodal volume. This flow is not represented in the head distribution because the fluid does not cross the edges of the nodal volume.

The three effects are included in the following manner:

1. The intermediate head values on a fracture are found from a linear interpolation between the fracture end nodes.

2a. If a diagonal fracture intersects a horizontal or vertical line through the particle, then the head at the intersection is found as in 1 above.

2b. If a fracture exists on the central row or column, then the head variation is assumed to be linear in the region of the particle.

3. A velocity term which is normal to the fracture is calculated for each fracture in the nodal volume. The term is found from the head rise in the volume which is not due to flow across the nodal edges. The velocity is assumed to decrease linearly to zero at the edge of the nodal volume.

4. A constant second derivative term is added to that calculated by the heads which are consistent with a linear decrease in velocity away from the fracture.

3.3.4 Particle Movement in Fractures. Particle travel in a given fracture begins at its injection, transfer from a matrix cell, or transfer from another fracture. Since each particle is traced for the duration of a computing interval, the time remaining in the interval is established at transfer into the fracture. Alternatively, if the previous computing interval was completed in the same fracture, the entire interval is available for the current move. In either case, the time remaining for the current move is known.

The initial conditions for the move, in addition to the time remaining in the increment, are the longitudinal and transverse positions of the particle in the fracture. The particle motion is due to longitudinal and transverse velocities and molecular diffusion. The final position, given the trajectory and time remaining, is in one of three potential hosts: the current fracture, the surrounding matrix, or a fracture junction. If the final position is in the surrounding matrix, the computation for this particle is placed in the matrix at its entry point and the remaining portion of the time increment spent in matrix travel. If the particle reaches a fracture junction during the interval it is transferred into the appropriate exit fracture, as subsequently described, and the remaining time spent in that fracture.

Laminar flow is assumed for all particle transport in fractures. The particle longitudinal advective velocity is determined from the mean (across the aperture) flow velocity. The Poiseuille velocity profile applies to the case of laminar flow between parallel plates. Therefore, the particle longitudinal velocity also depends on its lateral position. The Poiseuille velocity profile is given by:

$$v = 6\bar{v}\left[\frac{y}{b} - \left(\frac{y}{b}\right)^2\right]. \qquad (3.6)$$

In addition to a longitudinal velocity, particles have a deterministic transverse velocity which affects fluid transfer between fractures and the matrix. Both edges of the fracture may have different transverse flows. The transverse velocity is assumed to vary linearly from one edge to the other.

There are two terms which comprise the transverse flow in the fracture. These are flow leaving the fracture which accumulates in the nodal volume, and flow which leaves the fracture and subsequently flows from the nodal volume.

The fluid leaving fractures which does not accumulate in the matrix is found by finding the velocity due to the head gradient in the matrix just outside the fracture. The component of this velocity transverse to the fracture is used to determine the transverse velocity in the fracture. As an approximation, the velocity is calculated for each side of the fracture at the midpoint between nodes of the fracture and applied along the entire length.

The diffusive motion is selected, in Monte Carlo fashion, from a zero mean population with random orientation and an (independent) normally distributed standard deviation of

$$\sigma = (2D_m \Delta t)^{1/2} . \qquad (3.7)$$

The vector sum of the three displacements (longitudinal and transverse advection, diffusion) gives the trajectory, based on values at the beginning of the move.

The final model in the fracture travel regime is the transfer across a junction into another fracture. The model is constructed by tracing streamlines through the junction. In traversing a junction with multiple inlets and multiple exits, the particle is assigned an exit streamline which matches its inlet streamline in terms of flow differential from the origin of a circular flow scale around the junction (see Section 2).

3.3.5 Particle Release and Recovery. Tracer particles are introduced into the reservoir in the release subroutine. The release model simulates a continuous injection by releasing particles at random intervals over the designated release period. The number of particles released is calculated from the mass flow rate of tracer being injected.

There is no wellbore or injection path simulation in FRACSL. Instead a node is defined as the injection point. Particles are released from this node

into the matrix or into fractures. FRACSL selects fractures or the matrix randomly with a probability determined by fractional flow into each. In fractures, particles are placed across the fracture aperture using a probability function based on the Poiseuille velocity profile. Particles assigned to the matrix are placed at the radius of the wellbore at a uniformly random orientation.

Particles are withdrawn from the reservoir if they enter a designated recovery node from a fracture or approach within the well radius of the well node in the matrix. The average tracer concentration at the withdrawal node is calculated for the time step interval.

If desired, a message will be written to the output file whenever a particle is released or recovered. On release, the time of release, particle number, and initial position is output. On recovery, the time, number, and last position are recorded.

3.4 FRACSL Developments

Major improvements were made to the FRACSL code in three areas this past year. These improvements were made to make the code easier to use, to expand the capabilities so the code would be more versatile, and to eliminate areas where errors were introduced into the calculations. Many of the expanded capabilities were added for purposes of simulating the laboratory models.

3.4.1 Improvements.

3.4.1.1 Movement Error Control. To obtain the local pressure gradient at a particle position in the matrix, the pressures at the node nearest the particle and the eight adjacent nodes are used. These pressure values define a map which is a second order function of the x and y particle position. Both velocity and acceleration of the particle are determined from the map, and particle movement is determined by an Euler integration of the velocity and acceleration. Although acceleration is not constant with respect to particle position, particles are moved for a limited time with the assumption of constant acceleration.

The equations for acceleration in the x and y directions contain terms dependent on movement in the orthogonal direction. This makes development of an explicit solution for particle movement intractable. A reasonably efficient algorithm is attained by assuming constant acceleration over the time step. This is a considerable improvement over assuming constant velocity over a time step. The size of the time step is limited by an error criterion based on the rate of change of acceleration in space.

3.4.1.2 Fracture Impact on Matrix Movement. The conceptual basis for adjusting tracer movement in the matrix for the existence of nearby fractures was developed in 1984. However the details of implementing the algorithm in FRACSL were postponed due to time constraints. Planned simulations of the dual-permeability laboratory model required the code to account for fracture effects in the matrix.

The normal matrix flow velocity is calculated from a second order curve fit to the nine nearest nodal pressures. Local fractures act as barriers to the pressure distribution. The curve fit must be adjusted for the consequences of the barriers. In addition, there exists a flow component which is not accounted for in the nodal pressure representation. Fluid which leaves fractures and is stored in the matrix element, causing the nodal pressure to rise, is not represented in the pressure distribution. To model this flow, an additional flow is superimposed on the pressure dependent flow. This term decreases linearly with distance from the fracture which is consistent with fluid stored uniformly within the matrix element.

3.4.1.3 Multiple Matrix Properties. The ability to model varying matrix material is a requirement of any code which claims to be a general purpose tool. Rather than require that each matrix element be supplied with properties the FRACSL code allows the definition of a number of matrix types. Each type has specific properties and each element is defined to be a particular type.

3.4.1.4 Rectangular Channels. The modeling of the laboratory-scale fracture networks revealed that the infinite parallel plate assumption was too crude. The channels of the physical model are rectangular. Both the basic flow equation used to solve the hydraulics and the movement of tracer within a fracture were modified. The modification requires that the tracer position be calculated in three dimensions within the fracture. The particle input routine also was modified to be consistent.

3.4.1.5 Diffusion Limits. Investigations of the Raft River system revealed a modeling error in the code. It was found that far too much of the tracer

diffused out of fractures into the matrix. The model did not make any allowance for tracer particles striking the fracture walls. The code was modified such that particles have a probability of transferring to the matrix equal to the matrix porosity when they strike the fracture walls. The modification also allows the prohibition of particle transfers to the matrix which is useful in the laboratory model simulations.

Diffusion in the matrix was also reconsidered. The diffusivity in the matrix was reduced by a term called the geometric factor (Neretnieks, 1982). This term represents both the constrictivity of the matrix material and the tortuosity of diffusion within it. Constrictivity is the effect of particles bumping into the solid matrix in a like manner to the fracture considerations above. Tortuosity represents the extra movement a tracer particle must undergo in the matrix to move a given distance in the coordinate system. The geometric factor is defined as constrictivity divided by the square of the tortuosity.

3.4.1.6 Junction Function. A major addition to FRACSL this past year has been the development of an algorithm which determines the appropriate fracture and lateral position within that fracture to transfer a particle which reaches a fracture intersection. This algorithm is referred to as the junction function. Prior to incorporation of the junction function, complete mixing was assumed at fracture intersections. Laboratory studies at INEL have shown that very little mixing occurs under laminar flow conditions (Hull, 1985). The junction function can model fracture intersections under conditions of no, diffusion only, partial, or full mixing.

The junction function assumes laminar, streamline, viscous flow in a multibranch intersection of parallel-sided fractures. Transition zones, the length required for flow to reestablish the Poiseuille velocity profile, are on the order of two fracture widths and can therefore be neglected. An exact solution is found for the case of all inlet branches occurring in a continuous sequence around the intersection. A discontinuous case occurs when the inlet sequence is interrupted by an exit branch. The discontinuous case does not have a unique solution. The junction function forces a solution by assuming that the interrupting exit branch(s) is filled equally from the adjacent inlet branches. Once the nonmixing solution is determined, the desired mixing is added back using a random process.

3.4.2 New Capabilities.

3.4.2.1 Electrodes. The physical models used at INEL have electrodes implanted in them to measure tracer concentration at specific locations. An electrode model has been introduced into FRACSL which simulates the response of electrodes at regular intervals during a simulation. Electrode positions can be specified in the data input section of the code. A region around each electrode is scanned for the number of tracer particles existing within the region. The sum of the tracer mass in the region yields solute concentration in the region. The concentrations are written to a special file which allows plotting of time dependent concentration for each electrode.

3.4.2.2 Boundary Conditions. Boundary condition capabilities have been developed for FRACSL as the need arose. The initial boundary conditions developed were fixed external flow at each node. Using this boundary condition, the edges of a model are impermeable unless an external flow is specified. Fixed head boundary conditions could be used for steady state calculations by freezing the specific nodes in ACSL's ANALYZ routine. Not surprisingly more boundary conditions have been required.

Validation of the code for porous medium environments led to creation of a fixed head boundary condition outside the boundaries of the defined model. The model edges are connected to this fixed head via constant conductances. The conductances are calculated by determining the distance to the fixed boundary and assuming the material in-between is identical to the material surrounding the node. This boundary condition is appropriate for simulating a layer of infinite porous media with a single well and can be used for anisotropic materials.

Fixed external heads can be used for other situations. Fixed heads can be specified during transients at two definable nodes. These nodes were used to simulate a constant head source and sink for physical model experiments. Constant conductance connections to a zero head sink were developed for Raft River simulations. In these simulations, both fractures terminating at a model edge and nodes on the edge were connected to the sink by specifying the distance of the sink to each node. The code uses the matrix material or fracture aperture to determine the conductance.

3.4.2.3 Fracture System Synthesis. A two-dimensional fracture system synthesis capability

was added to FRACSL and used to develop the Raft River stochastic fracture system model presented by Miller et al. (1984). The synthesis follows the conditional probability model presented by Andersson et al. (1984). The synthesis is performed independently for multiple fracture sets, each with an assumed common orientation. Fractures are randomly placed along a normal scanline until the desired frequency is obtained. Fracture length is drawn from a lognormal random distribution. The distance of the fracture center from the scanline is uniform over the interval of half the sum of the fracture length and model height. Because the synthesis was developed for Raft River modeling, it contains some fixed statistics based on the Raft River RRGP-5 borehole.

3.4.3 Ease of Use Improvements.

3.4.3.1 Automatic Plotting Commands. One powerful feature of FRACSL is the ability to use high resolution graphics to study the results of simulations. Simulation data are written to a special file which is processed using the ISDMS graphics software installed at the INEL. The code allows plotting of pressure distributions, tracer particle distributions, electrode responses, and the tracer concentration returning to the well. The graphics package requires the data to be in a special format. Writing the data processing instructions required a substantial effort from the modeler. These commands are presently generated by the code based on the condition of a few user set flags. The generation of graphics is transparent to the user except for specifying file names and the actual plotting of the results. Plotting is not done automatically because the interactive plotting and data manipulation provides insight to the results.

3.4.3.2 Fracture Generation Routine. The fracture generation routine reduces the input burden on the modeler. One has the option of defining all fracture segments, or specifying all fracture segment groups which lay on a straight line regardless of length. In either case the input is checked for validity. Previously all segments had to be specified, which led to model errors for large fracture sets due to the difficulty of checking the input.

3.4.3.3 Grid Expansion. As the distance from the well increases, the detail required of the simulation decreases. A grid structure which expands with distance from the well takes advantage of this phenomena. Coding to generate an expanding grid structure has been added to FRACSL. The grid can be defined with four parameters rather than specifying each grid line.

3.4.4 User's Guide. The User's Guide was created to aid in both the use and review of the FRACSL code. It identifies all the options and necessary input to the code to minimize the support needed for modeler run simulations. The guide also contains the basis for the models developed for the code. The present version of the guide is both a reference document as well as a guide to using the code. The guide is not complete in either form or function. A major task of the next year will be to upgrade the document so that it can be useful outside of the Injection Program.

An addendum to the User's Guide has been created which is both innovative and highly useful. This is a nomenclature data base implemented on a microcomputer. The data base contains all variable names used in the code. These variable names were changed in the past year to conform with a standardized protocol. One can easily determine the meaning of nearly all the variables from the name alone using the protocol as a guide. The data base contains a wealth of information about the variables including size of arrays, default value, the task involved, where it is changed, each subroutine using the variable, and whether it is stored globally or locally. A short description of each variable is attached. The variables can be searched by name, task, subroutine, size, and need for specification by the user.

3.5 Code Validation

FRACSL is in the early stages of validation and the results have generally been encouraging. The code has been checked in unfractured media and against laboratory fracture models with no matrix conductivity.

3.5.1 Infinite Porous Media. Calculations have been compared to analytic results for a well injecting into an infinite layer of homogeneous porous material (Clemo, 1985). These comparisons were made for isotropic and anisotropic hydraulic conductivity situations. Both the pressure response and solute transport were investigated.

Pressure distributions for a constant drawdown rate were calculated for an isotropic conductivity condition and a conductivity nine times larger in the y direction than in the x direction. These

calculations were performed for a well at the center of the grid and repeated for a well at the corner of the grid with identical results. Hoopes and Harleman (1967) give the radial variation of head for an isotropic conductivity as:

$$\phi_{r_1} = \phi_{r_2} - \frac{Q}{2\pi zk} \ln \frac{r_1}{r_2} \quad . \tag{3.8}$$

The anisotropic case can be derived by transforming coordinates such that $x' = ax$ and $y' = y/a$. In the transformed coordinates, the conductivity is isotropic and Equation (3.8) applies with:

$$r_i = \sqrt{a^2 x_i^2 + y_i^2/a^2} \quad . \tag{3.9}$$

Dynamic pressure responses were calculated for the same conditions using the relationship given by Theis (1935):

$$\phi = \frac{2.3\ Q}{4\pi kz} \log 2.25 \frac{kzt}{r^2 S} \quad . \tag{3.10}$$

FRACSL was used to simulate East Mesa data (Clemo, 1985) using the parameters in Table 3.1. An explanation of the chosen parameters can be found in the FRACSL User's Guide (Clemo and Miller, 1985).

For steady state conditions, the infinite porous media was simulated using a boundary condition option which assumes the reservoir parameters extend to a zero head ring, with dimensions appropriate to the conductivity anisotropy. The ring was set at an effective radius r_i of 200 ft.

Table 3.2 presents the results for the constant drawdown case. It shows superb agreement of FRACSL with the analytic solutions. Table 3.3 presents results of the dynamic simulations at a distance of 15 ft from the well.

Solute transport was simulated for steady-state flow conditions. A slug tracer injection test was simulated for isotropic conductivity conditions. The dispersivities were set to zero which resulted in an expanding circle of tracer particles. The radial position of the particles is given by:

$$\bar{r} = \sqrt{\frac{tQ}{z\pi\xi} + r_{well}^2} \quad . \tag{3.11}$$

Table 3.4 presents the results of these simulations in comparison to Equation (3.11).

Table 3.1. FRACSL model parameters

Model size:	150 x 150 ft (11 x 11 nodes)
Hydraulic conductivity:	7.9 ft/day or 23.7 ft/day in y direction and 2.63 ft/day in x direction
Storage coefficient:	1×10^{-5}
Porosity:	0.25
Thickness:	1 ft
Flow rate:	462 ft^3/day

The uncertainty given in the FRACSL results is the standard deviation of the particle position about the given radius. The particle deviations are preferential with greater errors along the axes and diagonals of the grid. The small deviation at 0.05 days is due to special handling of the region near the injection well. The delay and recovery of the particles at 0.25 days and 0.55 days, respectively, is due to the coarse nodalization.

Table 3.2. Comparison of FRACSL and analytic drawdowns

Isotropic Case

r (ft)	Analytic Drawdown (ft)	FRACSL Drawdown (ft)	Error (%)
15	24.55	24.11	-1.8
45	14.00	13.88	-0.8
90	7.46	7.43	-0.4
212	-0.49	-0.54	-10.2

Anisotropic Case

x (ft)	y (ft)	r (ft)	Analytic Drawdown (ft)	FRACSL Drawdown (ft)	Error (%)
0	15	8.7	32.15	31.93	-0.7
45	0	77.9	11.70	11.63	-0.6
0	150	86.6	10.72	10.84	+1.1
150	0	260.0	0.49	0.46	-6.1

Table 3.3. Comparison of dynamic pressure response

	Isotropic Conductivity		Anisotropic Conductivity			
			Low Conductivity Direction (x)		High Conductivity Direction (y)	
Time (days)	Analytic Pressure (ft)	FRACSL Pressure (ft)	Analytic Pressure (ft)	FRACSL Pressure (ft)	Analytic Pressure (ft)	FRACSL Pressure (ft)
0.0	0.0	0.0	0.0	0.0	0.0	0.0
0.01	20.32	20.36	15.21	14.62	25.43	24.64
0.02	23.54	23.56	18.43	17.78	28.65	27.84
0.05	27.80	27.83	22.69	22.04	32.91	32.13
0.08	29.41	30.01	24.88	24.38	35.09	34.48

A second transport test accounting for dispersion was run with continuous particle injection. The longitudinal dispersivity was 0.6 ft and the transverse dispersivity was 0.2 ft. Bear (1972) defines the dependence of concentration on radial distance traveled by:

$$C/C_o = 1/2 \text{ erfc}\left(\frac{r - \bar{r}}{4/3D_L r}\right) . \quad (3.12)$$

Figure 3.4 shows C/C_o as a function of distance from the well and shows an excellent match to the theoretical results. The results indicate that the deviations about the nominal radius, apparent in Table 3.4, are small compared to the dispersive term. In Figure 3.4 the variability of the concentration near the well is a property of dispersion for the limited number of tracer particles used in the simulation.

Table 3.4. Comparison of tracer slug transport

Time (days)	Analytic Radius (ft)	FRACSL Radius (ft)	Error (%)
0.0	0.0	0.0	0.0
0.05	5.46	$5.44 \pm 1 \times 10^{-5}$	-0.4
0.25	12.13	11.87 ± 0.3	-2.1
0.55	17.99	17.99 ± 0.4	0.0
1.05	24.84	24.21 ± 0.5	-2.6
2.05	34.73	34.23 ± 0.7	-1.4

3.5.2 East Mesa. Tracer injection and recovery tests at the East Mesa Known Geothermal Resource Area (KGRA) in the Imperial Valley have provided a data set with which to examine FRACSL's ability to match data from a porous reservoir. The layering of sandstone and shale in East Mesa provided a very low vertical permeability. Flow out of the two injection wells tested at East Mesa was predominantly two-dimensional in nature which is easily modeled by FRACSL.

The FRACSL model described a single representative layer of the sandstone with homogeneous material properties. Both pressure dynamics and tracer recovery at the wellhead were simulated. The wellbore pressure response data from East Mesa has not been matched by the FRACSL simulations. The pressure response at East Mesa showed a transition from one established time constant to another; whereas the FRACSL model showed only a single time constant. The two period nature of the East Mesa well response has not been explained.

The tracer tests at East Mesa consisted of a 12 h injection of tracer material, a 12 h quiescent period, and finally a withdrawal period of sufficient length to recover nearly all of the injected tracer. These tests were conducted at the two wells with

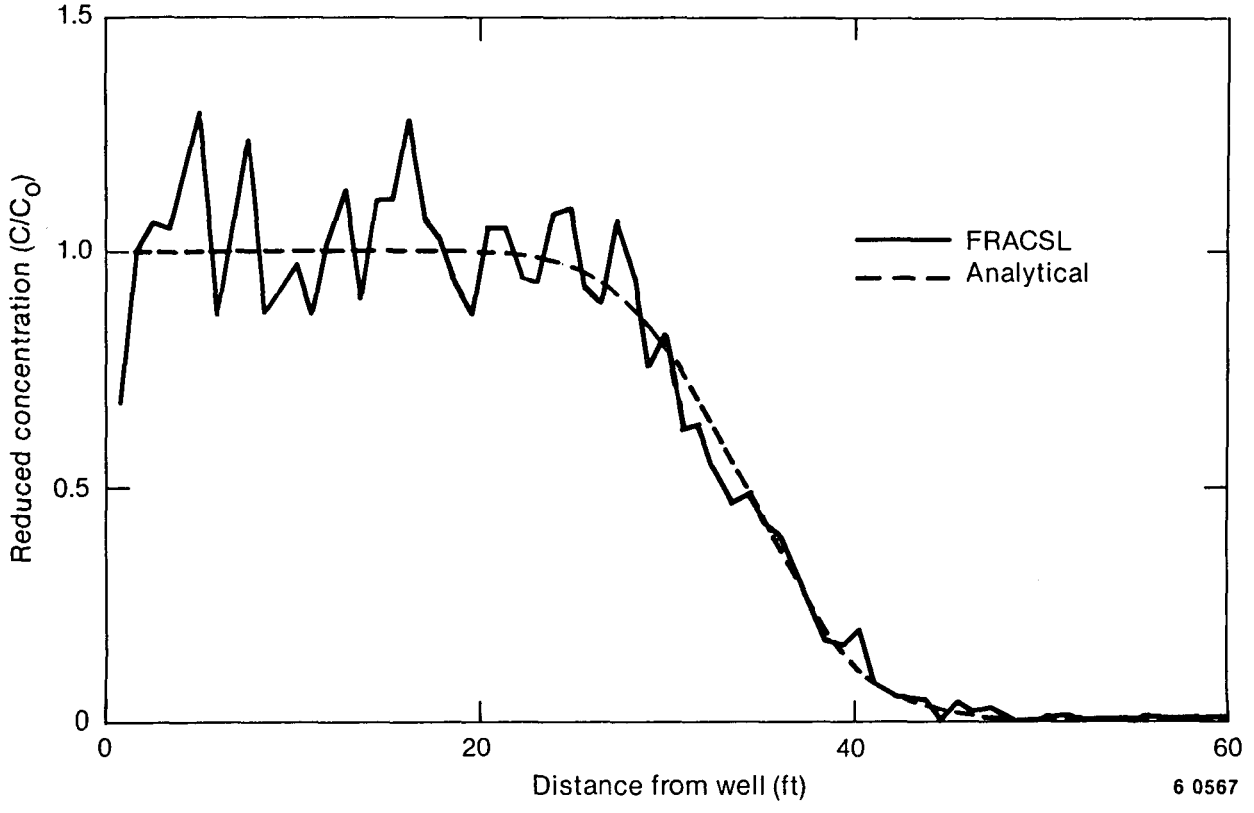

Figure 3.4 Comparison of dispersion of FRACSL simulation to an analytical solution for radial flow from a well.

varying flow rates. In a second test series, the quiescent period was lengthened to 6 mo for one test at each well. For each test, a 5 min pulse of a different tracer material was injected along with the continuous tracer.

Each of the short quiescent tests were matched by adjusting the dispersivity coefficient in FRACSL until the simulated tracer recovery was deemed in agreement with the measured data. Figure 3.5 is an example of a typical match of tracer recovery. The ordinate is normalized by the total fluid volume injected and the abscissa is normalized by the injection concentration. The solid FRACSL line is a seventh order curve fit to the FRACSL simulation result. The deviations at the ends of the line are a result of the curve fitting process. It was found that all of the short quiescent tests could be matched by a single dispersivity coefficient for each well. This was true for both slug and continuous tracer.

In one of the tests with a long quiescence, the tracer material was not recovered after 18 injection volumes of withdrawal. In the other well, nearly all of the tracer had been recovered after 16 injection volumes. In this test the tracer concentration peaked at 7.5 volumes recovered. One possible explanation of these two occurrences is the existence of natural drift in the East Mesa reservoir.

The hypothesis was investigated using the FRACSL code. A match could be accomplished with a natural drift and the same dispersivity used in the short quiescent tests. The match required an anisotropic hydraulic conductivity with nine times the conductivity in the direction perpendicular to drift than in the drifting direction. Figure 3.6 shows the FRACSL simulated recovery with these conditions along with data from East Mesa.

The comparisons made with the East Mesa test data do not constitute a verification of the FRACSL code. However, when viewed in conjunction with comparisons to analytical porous media results, the matches made to tracer recovery data reveal the power available in FRACSL to study tracer testing in an unfractured reservoir.

3.5.3 Fracture Systems. Simulations using the FRACSL code have been compared to analytical solutions for transport in single fractures, and laboratory data collected from physical models.

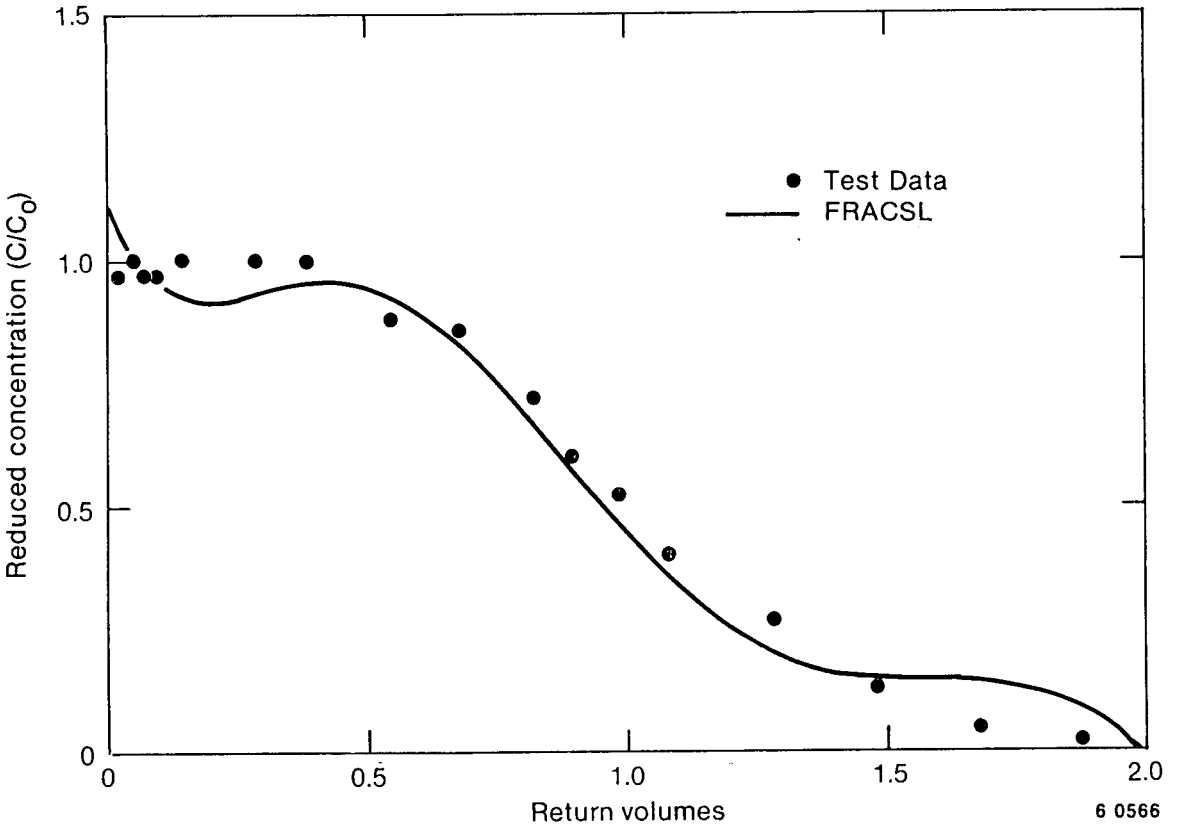

Figure 3.5 East Mesa test, continuous tracer injection.

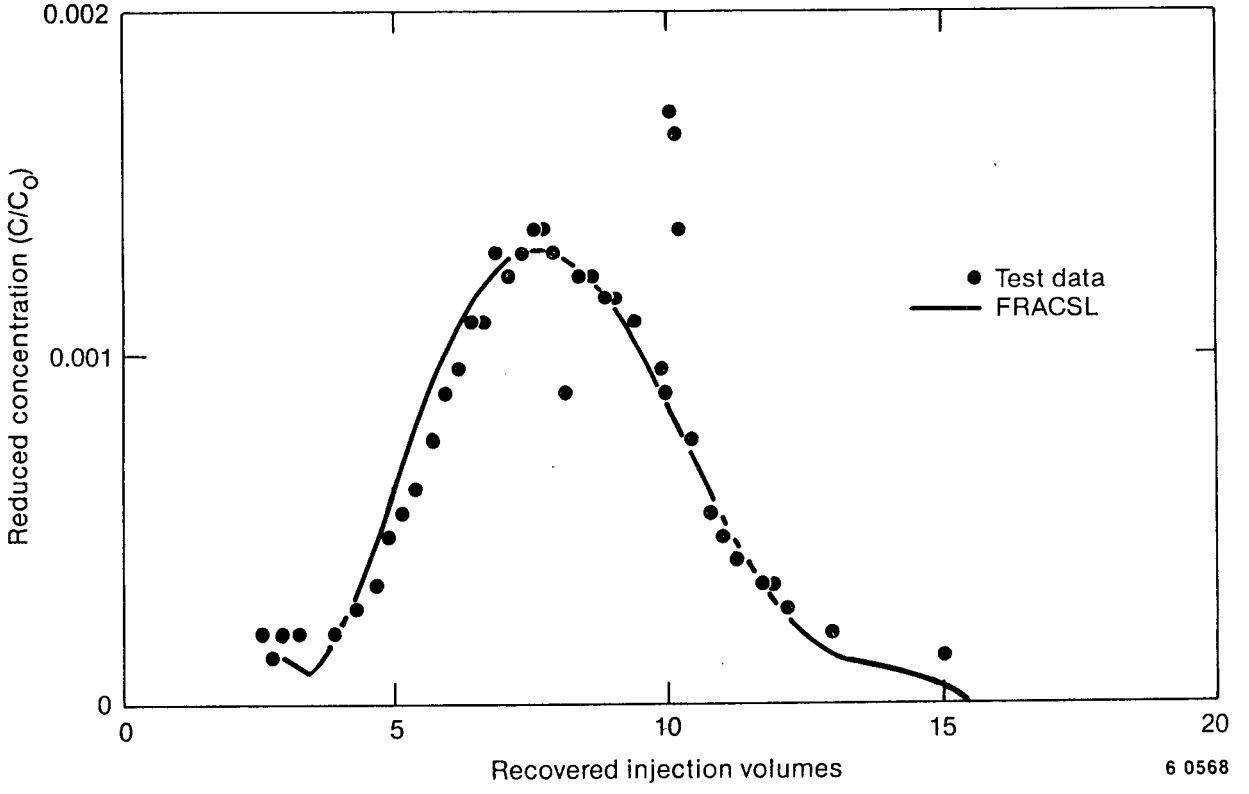

Figure 3.6 Response to five minute tracer slug, Well 56-30 six-month quiescent test.

Analytical solutions for breakthrough of a tracer at the end of a fracture can be derived for high flow rates (velocity profile only) and very low flow rates (diffusion homogenizes tracer across the fracture).

Figures 3.7 and 3.8 shown comparisons between computer simulations of tracer breakthrough and theoretical results. Breakthrough is the volumetrically averaged solute concentration passing a given point. These figures show that the algorithm accurately simulates the important relationship of fluid velocity and dispersion coefficient. The relationship is contained in the Peclet number (Pe), which is the ratio of the fluid velocity times the distance traveled in the fracture to the dispersion coefficient.

Figures 3.9 through 3.12 are comparisons of simulated tracer breakthrough to breakthrough measured from a single fracture laboratory model. If one compares the difference of the simulated-to-measured curves to the differences between figures, it becomes obvious that the random-walk algorithm simulates the important phenomena of dispersion in parallel-sided fractures.

To validate the fracture flow portion of the FRACSL code, a comparison was made between an analytical equation for flow in fractures, data from the laboratory fracture model, and FRACSL simulations. Because the laboratory model is comprised of rectangular channels, not infinite parallel plates, the appropriate flow equation was used (Happel and Brenner, 1965):

$$Q = \frac{\rho g}{24\mu}\frac{d\phi}{dx}\left[ab(a^2+b^2) - \frac{192}{\pi^5}\cdot\sum_{n=1}^{\infty}\frac{1}{(2n-1)^5}\left(a^4\tanh\frac{2n-1}{2a}\pi b + b^4\tanh\frac{2n-1}{2b}\pi a\right)\right]. \quad (3.13)$$

Figure 3.13 shows the effect of decreasing aspect ratio on discharge through a rectangular channel. At an aspect ratio of 6 to 1 for the physical model, there is a 10% decrease in discharge through the rectangular channel compared to parallel plates.

Equation (3.13) was used to calculate head loss versus discharge for fractures in the physical model. This head loss was then multiplied by the number of fractures in the length of the model. This assumes that the fracture network can be replaced by a single fracture of equivalent length, and that there are no head losses at fracture junctions (Wilson and Witherspoon, 1976).

Flow tests were conducted on the fracture network physical model (see Figure 2.6) in the laboratory. The network consists of two sets of orthogonal fractures, all of equal aperture and height. Twenty-one fractures separated the two piezometers used to measure head. Flow was measured by collecting and measuring the volume of water discharged over a given time interval. Because the fractures are fairly wide (3.2 mm), the conductivity of the model is large, and the head loss across the model is small. Figure 3.14 shows a plot of head loss as a function of discharge for the physical model. The maximum head differential measured was only 6.8 mm. Because of hysteresis effects in the piezometer tubes, there is about a u1 mm uncertainty in the head measurements.

Also shown in Figure 3.14 is the analytical solution for flow in rectangular channels. Solving Equation (3.13) for a = 1.905 cm, b = 0.3175 cm and 20°C gives:

$$Q = -440.2\,\frac{d\phi}{dx}\,cm^3/s \quad . \quad (3.14)$$

A least square regression through the data points gives:

$$Q = -430.5 \pm 21.6\,\frac{d\phi}{dx}\,cm/s$$

(95% confidence interval) . (3.15)

There is no significant difference between the regression equation and the analytical solution. Both curves plot on top of each other in Figure 3.14. Therefore, it is concluded that there are no significant head losses due to the 21 fracture junctions between the two piezometers used to measure head loss.

FRACSL simulations of the model were made for discharge rates of 200, 400, and 600 cm^3/min. Predicted head losses are plotted in Figure 3.14 as circles. The difference between the analytical solution results and the FRASL results is less than 0.25%.

FRACSL accurately matches the analytical solutions for flow in fractures based on the parallel plate theory. It also matches measured head losses from the laboratory physical model. No evidence

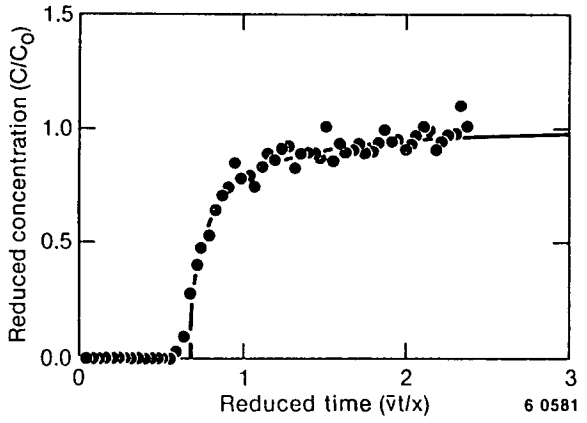

Figure 3.7 Comparison of analytical (line) to numerical (points) solutions for tracer breakthrough where dispersion is controlled by the parabolic velocity profile (Pe = 0.0).

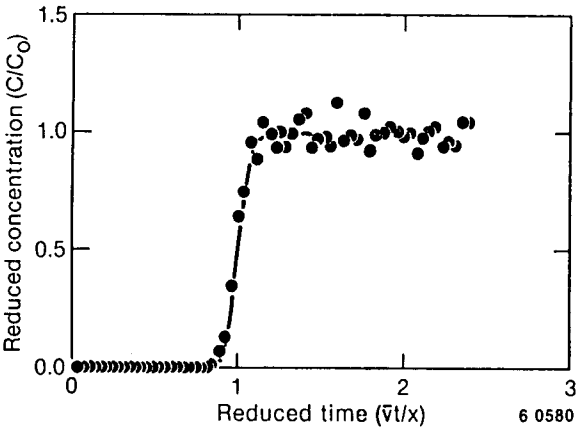

Figure 3.8 Comparison of analytical (line) to numerical (points) solutions for tracer breakthrough where transverse molecular diffusion dominates development of a parabolic velocity profile (Pe = 500).

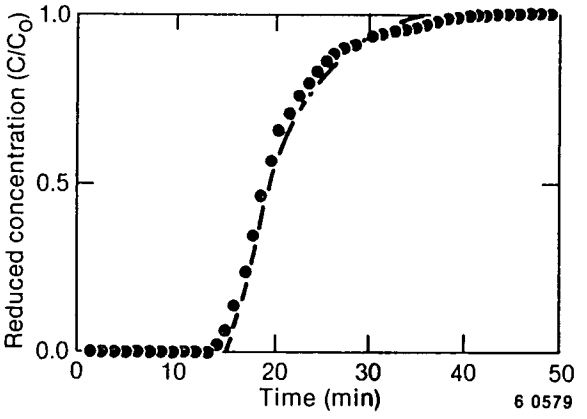

Figure 3.9 Comparison of tracer breakthrough measured in the single-fracture laboratory model (line) with simulated breakthrough (points) at an average flow velocity of 3.0 cm/min.

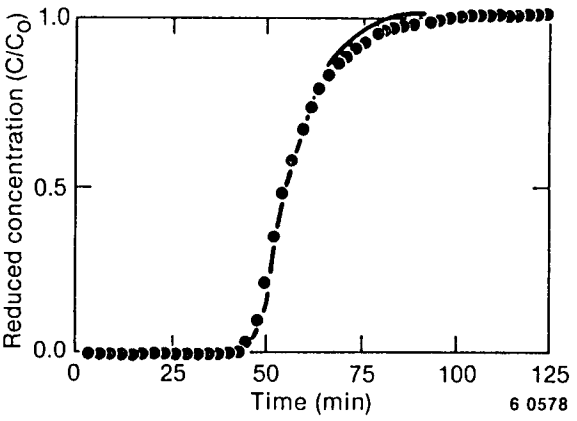

Figure 3.10 Comparison of tracer breakthrough measured in the single-fracture laboratory model (line) with simulated breakthrough (points) at an average flow velocity of 1.0 cm/min.

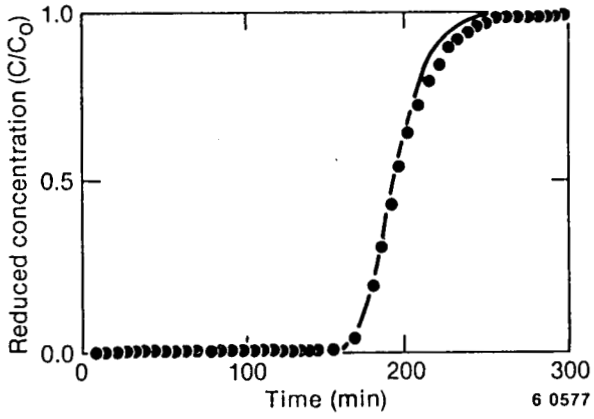

Figure 3.11 Comparison of tracer breakthrough measured in the single-fracture laboratory model (line) with simulated breakthrough (points) at an average flow velocity of 0.3 cm/min.

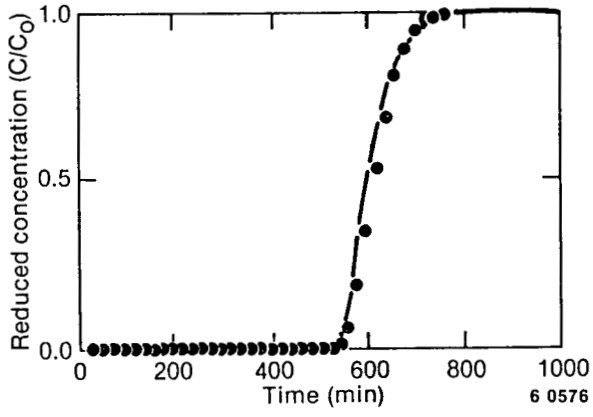

Figure 3.12 Comparison of tracer breakthrough measured in the single-fracture laboratory model (line) with simulated breakthrough (points) at an average flow velocity of 0.1 cm/min.

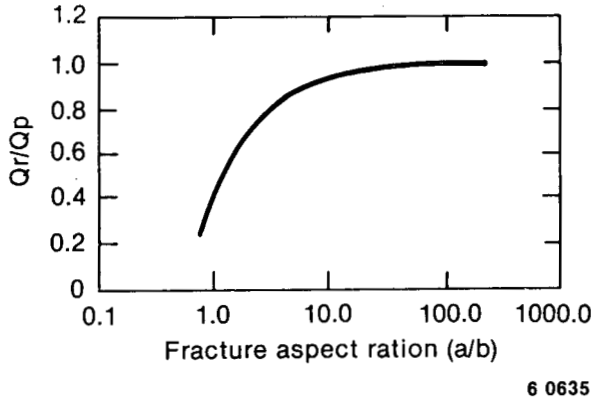

Figure 3.13 Ratio of discharge through a rectangular channel to discharge through parallel plates having the same aperture and cross-sectional area.

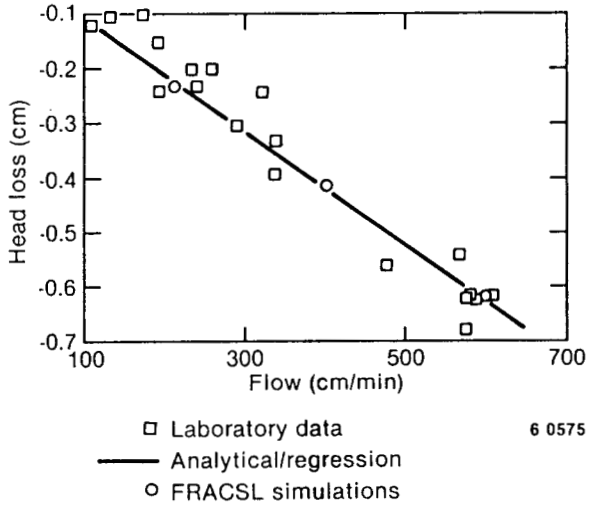

Figure 3.14 Head loss in the physical model as a function of flow rate.

of interference effects at fracture junctions was found for a network consisting of 192 fracture elements.

3.6 Conclusions

The FRACSL code has the capability to simulate fluid dynamics and tracer solute transport in a fractured, isothermal two-dimensional reservoir. Within the limits of the present configuration, the major elements of the code have been finalized. Use of the code has led to revisions to meet the needs of new applications. The code has been used in all of the environments for which it was initially designed, and has met the needs of those applications. New applications within these environments will certainly require added capabilities to simulate unique situations.

Considerable effort was expended in the past year to make FRACSL more efficient and easier to use. These changes have reduced the cost of individual simulations, and the time required to set up a model. The most significant development has been the User's Guide and the nomenclature data base. These documents must be developed further, but have already proved their usefulness.

FRACSL has shown good agreement with theory and laboratory data for the conditions against which it has been tested. These conditions include isotropic and nonisotropic homogeneous porous media and fracture networks. The code needs to be further validated in the dual-permeability domain before it can be fully utilized for reservoir simulation.

3.7 References

S. W. Ahlstrom, H. P. Foote, R. C. Arnett, C. R. Cole, R. J. Serne, *Multicomponent Mass Transport Model: Theory and Numerical Implementation* (Discrete-Particle-Random-Walk Version), BNWL-2127, 1977, Pacific Northwest Laboratory, Richland, WA.

J. Andersson et al., "A Stochastic Model of a Fractured Rock Conditioned by Measured Information," *Water Resources Research, 20*, 1, 1984, pp. 79-88.

T. M. Clemo "FRACSL Code Development and Correlation of East Mesa Test Results," *Tenth Workshop on Geothermal Reservoir Engineering, SGP-TR-84, Stanford University, 1985*, pp. 287-292.

T. M. Clemo and J. D. Miller, *Fractured Media—Advanced Continuous Simulation Language (FRACSL) User's Guide*, EG&G Idaho Internal Report, Idaho National Engineering Laboratory, 1985.

J. Happel and H. Brenner, *Low Reynolds Number Hydrodynamics*, Englewood Cliffs, NJ: Prentice-Hall Inc., 1965.

J. A. Hoopes and D. R. F. Harleman, "Dispersion in Radial Flow From a Recharge Well," *Journal of Geophysical Research, 72* 14, 1967, pp. 3595-3607.

L. C. Hull, *Physical Model Studies of Dispersion in Fracture Networks*, EGG-ELS-6845, Idaho National Engineering Laboratory, 1985.

J. D. Miller et al., *Raft River Characterization and Reservoir Simulation*, SE-PB-84-058, Idaho National Engineering Laboratory, 1984.

Mitchell and Gauthier Associates, *Advanced Continuous Simulation Language (ACSL) User's Guide and Reference Manual*, Mitchell and Gauthier Assoc., P.O. Box 685, Concord MA, 1981.

Ivars Neretnieks, "The Influence of Microfissures in Crystalline Rock on Radionuclide Migration," *Predictive Geology With Emphasis on Nuclear-Waste Disposal*, G. DeMarsily and D. Merriam (eds.), 1982, pp. 137-152.

T. A. Prickett, T. G. Naymik, and C. G. Lonnquist, "A 'Random-Walk' Solute Transport Model for Selected Groundwater Quality Evaluations," *Bulletin 65*, Illinois State Water Survey, Champaign, IL, 1981.

E. S. Romm, *Fluid Flow in Fractured Rocks*, Moscow, Nedra (in Russian), 1966.

C. R. Wilson, and P. A. Witherspoon, "Flow Interference Effects at Fracture Intersections," *Water Resources Research, 12* 1, 1976, pp. 102-104.

4. DEVELOPMENT AND APPLICATION OF TRACERS: EXAMPLES OF FIELD AND EXPERIMENTAL STUDIES

Michael C. Adams and Joseph N. Moore
Earth Science Laboratory
University of Utah Research Institute
Salt Lake City, UT

4.1 Introduction

The ideal tracer should be detectable in small quantities, inexpensive, environmentally safe, and be absent from natural geothermal fluids and groundwaters. The tracers currently in use in high-temperature environments fall into three major categories: (a) isotopes; (b) salts of iodide, bromide, or chloride; and (c) organic dyes. Each of these classes of tracers has significant limitations. Isotope tracers, although inert, are difficult to handle, expensive to analyze, potentially environmentally hazardous, and once used, contaminate the reservoir for long periods of time. The salts, while relatively stable and inexpensive, nonetheless may be adsorbed by the reservoir rocks. In addition, because of the abundance of chloride in most geothermal waters, large quantities of chloride tracers are necessary. Relatively little is known about the organic dyes. Fluorescein and rhodamine are the most commonly used. However, fluorescein is light sensitive and these dyes, like the salts, may be adsorbed. Their stability at geothermal temperatures is variable. For instance, in a recent two-well injection test at Svartsengi, Iceland, only 4% of the dye rhodamine WT and 30% of the iodide were recovered after 5 months (Gudmundsson et al., 1984). Since the tracers were injected together, these relationships suggest that the dye probably decomposed underground. The data indicate zero order decay of the dye.

In addition to these limitations, the relatively small number of tracers available restricts the number of wells that can be individually monitored in a producing field at any one time. Thus, in geothermal fields where many injection wells are in use, it is not yet possible to independently trace the movement of fluids injected into each of them.

The fluorinated and sulfonated hydrocarbons are a relatively new class of tracers that do not appear to suffer from many of these disadvantages. These compounds have been used as tracers in groundwater studies in low temperature environments but have not yet been field tested at high temperatures. Some of them are, however, expected to be stable at high temperatures.

The fluorinated hydrocarbons are produced by substituting fluorine for hydrogen in organic molecules. Thus, a large number of different fluorinated hydrocarbons, which vary regularly in their chemical and physical properties (i.e., a homologous series) can be produced. Because the properties of the individual compounds are similar, the geothermal fluids can be analyzed for all of the components in the series simultaneously by chromatography. These compounds have the additional advantage of being detectable in extremely small quantities. Using presently available technology, the fluorinated hydrocarbons can be detected in concentrations in the parts per billion range, and it appears likely that detection limits of several tens to hundreds of parts per trillion are feasible. Although dilution factors between wells will probably vary greatly from place to place, it can be assumed that only minute amounts of tracer will be present during the initial breakthrough of the injected brine. For example, dilution factors of 10^8 have been measured in the Wairakei geothermal field. Current detection limits of the fluorinated hydrocarbons are compatible with dilution factors of this magnitude. Furthermore, fluorinated hydrocarbons are absent from natural waters and they can be designed to partition in either the gas or the liquid phase of a geothermal fluid, allowing the possibility of investigating both components of a two-phase system separately. In addition to the fluorinated hydrocarbons, several sulfonated hydrocarbons will be tested because they perform well as groundwater tracers.

4.2 Experimental Procedures

Four experimental reaction vessels were put into operation during 1985 to determine the stabilities of the organic dyes, fluorescein and rhodamine,

and selected hydrocarbons. These vessels are housed at the University of Utah's Department of Metallurgy and are dedicated solely to the tracer stability investigations. A fifth vessel capable of sustaining temperatures of up to 350°C is currently being fabricated and should be installed prior to the end of FY-1985. The use of multiple reaction vessels makes it possible to perform experiments of relatively long duration (days to weeks) on several different tracers or under different conditions simultaneously.

At the beginning of each experiment, aliquots of the solutions containing the tracer are encapsulated in sealed quartz tubes (Figure 4.1). The ampules are filled with approximately 30 mL of solution and sealed in an oxygen-methane flame. At least 2 mL of the ampule are occupied by a gas phase during each experimental run. The gas phases used for these experiments are pure nitrogen or an atmospheric mixture of oxygen and nitrogen which is approximately 20% oxygen by volume. These gas phases were chosen as end-members to bracket the variable oxidation potentials produced by different surface treatments during injection.

The solutions for the experimental runs that used a nitrogen gas phase were purged with nitrogen gas in the ampule for up to 2 h. The neck of the ampule (see Figure 4.1) was aspirated to prevent oxygen contamination from the oxymethane flame during sealing.

Three ampules can be tested within each reaction vessel. Under normal experimental conditions the reaction vessels are heated to the desired temperature within 3 h. During long experimental runs, the reaction vessel can be brought back to ambient temperature to remove individual ampules and then reheated. Cycling the temperatures in this way can be done rapidly, in less than 6 h. By keeping the duration of the experimental run at least ten times the duration of the heating and cooling cycles, adverse chemical effects are minimized. Chemical analyses of the solutions are performed both before and after each experiment to evaluate the reactions and conditions during the test.

4.3 Experimental Results

The experimental runs were designed to evaluate the effects of four different parameters: temperature, time, solution chemistry, and the partial pressure of oxygen. To date, the investigations have centered on the stability of fluorescein, three fluorinated hydrocarbons, and two sulfonated hydrocarbons. These experiments have been conducted at temperatures ranging from 100 to 200°C. The hydrocarbons tested were:

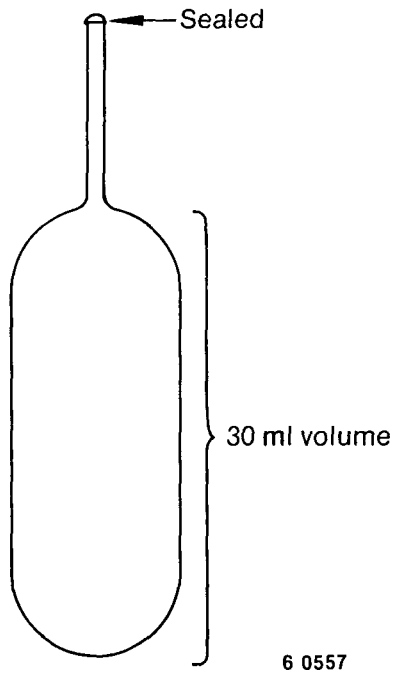

Figure 4.1 Illustration of quartz tube used for hydrothermal experiments.

- a-, a-, a- trifluoro-m-toluic acid
- p - fluorobenzoic acid
- pentafluorobenzoic acid
- p - toluenesulfonic acid
- benzenesulfonic acid.

The factors investigated with fluorescein can be divided into destabilizing and stabilizing factors. Increasing oxygen pressure and temperature have a destabilizing effect. These effects are shown in Figures 4.2 and 4.3. Inspection of these figures shows that the presence of oxygen in the gas phase is the major destabilizing effect. The initial tracer concentration of 5 ppm was reduced to less than 0.05 ppm in 20 h with oxygen (Figure 4.2), while the nitrogen runs show little degradation even at

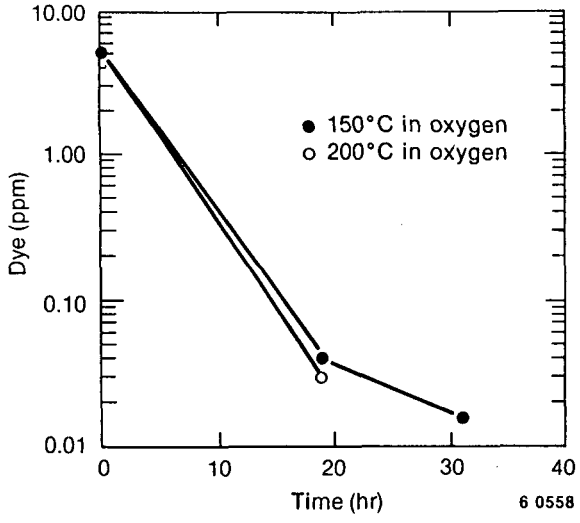

Figure 4.2 The effect on fluorescein stability of atmospheric oxygen in the gas phase at 150°C and 200°C. The initial fluid phase contained 825 ppm NaCl and 5 ppm fluorescein.

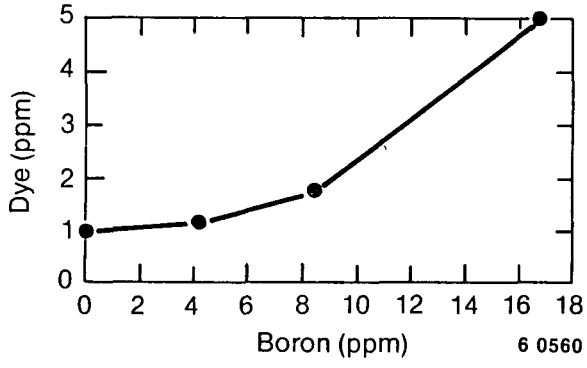

Figure 4.4 The effect of aqueous boron on the stability of fluorescein. The run temperature was 150°C. The initial fluid phase contained boron, 825 ppm NaCl, and 5 ppm fluorescein. The pH was buffered to ∿ 6.5.

90 h (Figure 4.3). The effect of temperature is so small between 150 and 200°C that it is within the experimental error.

The stabilizing factors found to date are boron and boron + pH. The effects of boron are illustrated in Figure 4.4 where a solution with an initial concentration of 5 ppm fluorescein was run for 118 h at 150°C. The composition of the gas phase during this experiment may have contained some oxygen, as indicated by the low concentrations of fluorescein in the 0 to 8 ppm boron runs. However, the trend of increasing stability with increasing boron is clear. The effect of increasing pH on fluorescein stability is shown in Figure 4.5. During this experiment the pH was buffered with boric acid and sodium borate. Thus the dramatic increase in stability between pH 7 and 8 could be due to pH-dependent changes involving either boron or fluorescein. Since borates change species at a pH of ∿9, phenol groups at 6 to 7.5, and carboxyl groups at 4 to 6, the pertinent disassociation is probably the phenol group on the fluorescein molecule.

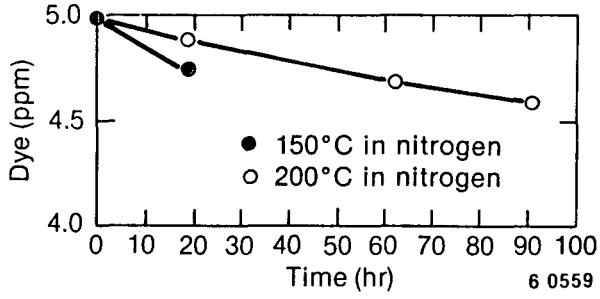

Figure 4.3 The effect on fluorescein stability of purging the gas phase with nitrogen.

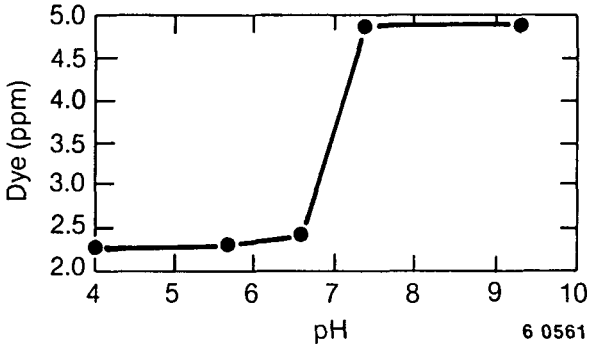

Figure 4.5 The effect of buffering fluorescein solution pH with boric acid and sodium borate. The run temperature was 150°C. The initial solution contained 825 ppm NaCl and 5 ppm fluorescein.

This conclusion is supported by an experimental run at high pH without boric acid/sodium borate buffering. In this run, the solution was geothermal brine (boron = 1.0 ppm, pH = 8.7). The fluorescein was only reduced to 4.8 ppm from an initial value of 5.0 ppm after being heated to 200°C for 92 h.

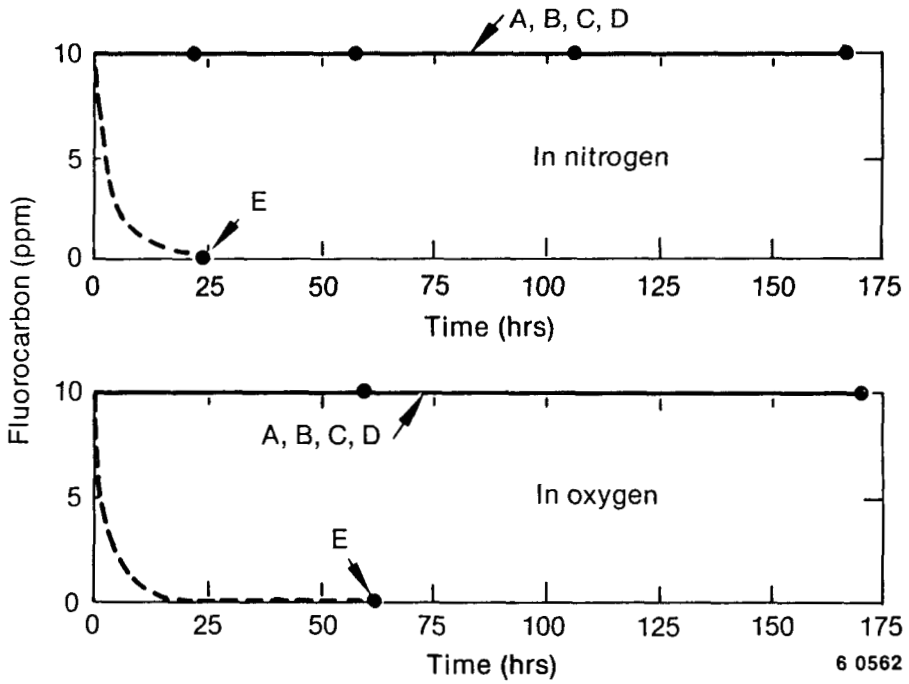

Figure 4.6 The stability of fluorinated hydrocarbons and phenyl-sulfonates at 125° and 150°C in the presence of an oxygen or nitrogen gas phase. Compounds A to E are p-fluorobenzoic acid (A), α-, α-, α-trifluoro-m-toluic acid (B), p-toluenesulfonic acid (C), benzenesulfonic acid (D), and pentafluorobenzoic acid (E).

Plans for future higher temperature experiments using fluorescein are to use various geothermal brines as solvents as well as distilled water, rather than parameterizing the effect of each solution component. This approach will be taken because (1) the separate compositional dependence of fluorescein on each element in a geothermal brine is beyond the scope of this project, and (2) geothermal brine compositions are limited to a relatively narrow range of elemental ratios.

There may be other compositional factors in addition to those tested to date. If this is the case, then the runs using geothermal brine as a solvent will produce significantly different results. In this case the approach will be modified.

The initial stability tests on fluorinated and sulfonated hydrocarbons were very encouraging. Solutions containing all five of the hydrocarbons at an initial concentration of 10 ppm each were run for up to 174 h at temperatures of 125 and 150°C in oxygen and in nitrogen. The only compound to detectably decay was pentafluorobenzoic acid (Figure 4.6). The decay of pentafluorobenzoic acid was complete and occurred at all temperatures, times, and in all gas phases. These experiments will be repeated in geothermal brines and at higher temperatures.

4.4 Field Applications

Tracers were used by UURI to monitor the scaling behavior of silica and calcium during injection tests at the East Mesa geothermal field (Adams, 1985). The major and minor cations and anions in the fluids were also monitored during these tests.

Figures 4.7 and 4.8 show the concentrations of Ca and SiO_2 in the fluid being withdrawn after injection. The horizontal axis is in units of the volume of injected fluid. The dashed line in these figures, or recovery curves, represents the concentration that would occur in the fluid if no water-rock reaction had occurred. The solid line represents the actual concentration measured in the fluid.

Two wells were tested at East Mesa, Wells 56-30 and 56-19. The tests are referred to below by their test number with the test well in parentheses.

4.4.1 Ca and SiO_2 Behavior. During the injection-backflow tests at East Mesa, both Ca and SiO_2 were lost during injection. Inspection of the recovery curves in Figures 4.7 and 4.8 shows that, in most cases, minerals that precipitated during

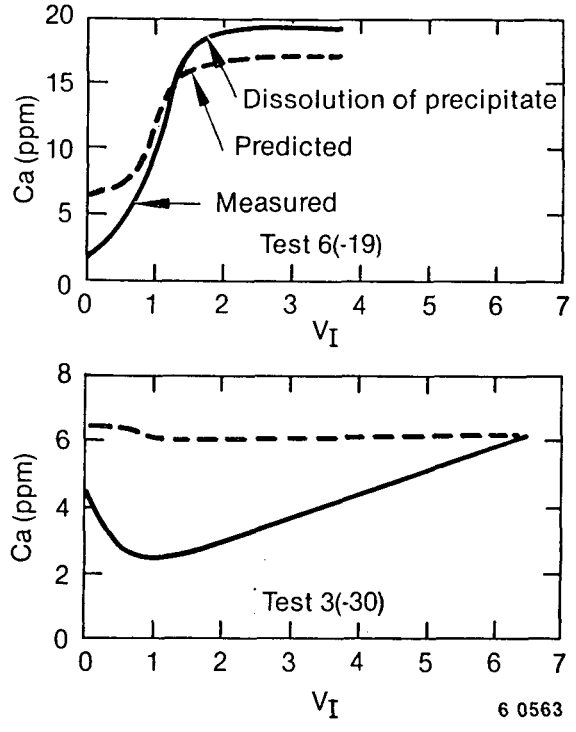

Figure 4.7 Recovery curves contrasting the behavior of Ca in Wells 56-19 and 56-30. Dashed lines are predicted concentrations and the solid lines are measured concentrations. V_I = the volumes of injectate recovered.

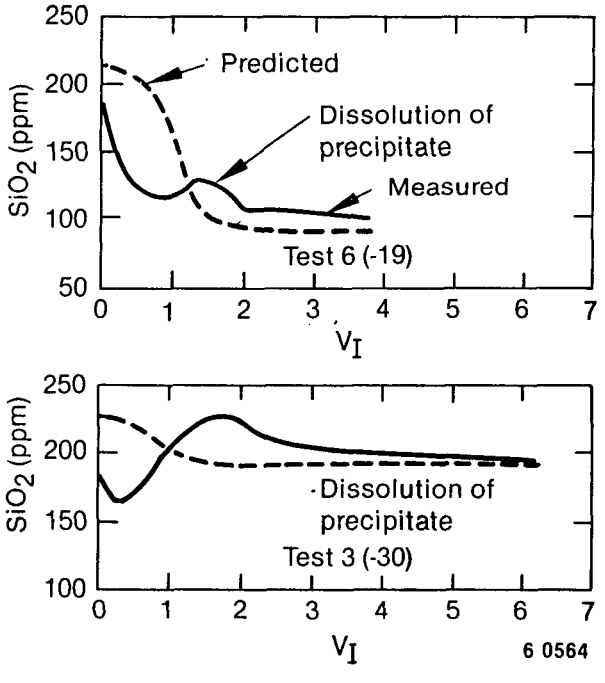

Figure 4.8 Recovery curves contrasting the behavior of SiO_2 in Wells 56-19 and 56-30. See Figure 4.7 and text for explanation.

injection were then dissolved after the unmixed body of injectate had been recovered. The only case where this did not occur was during Test 3(-30) (Figure 4.7). During this test aqueous Ca concentrations were reduced to as low as 30% of the injected concentration. In addition, reservoir Ca concentrations did not return to the background value of 6.0 ppm until 6.5 injection volumes had been recovered. The prolonged precipitation of Ca from the reservoir fluid in Well 56-30 may have been due to the attainment of critical nucleation size or may simply be related to the degree of supersaturation in the fluid.

The maximum amount of Ca precipitation in Well 56-30 (Figure 4.7) occurred at least 0.6 injection volumes away from the wellbore (Michels, 1983). However, the maximum Ca precipitation during Well 56-19 tests occurred adjacent to the wellbore. Thus it appears that, unlike the behavior of Ca in Well 56-30, the scale inhibitor failed to prevent near-well borehole precipitation in Well 56-19.

It has been suggested by Fournier (1981) that chalcedony should be considered as the equilibrium SiO_2 polymorph for geothermal systems with temperatures below 180°C. Despite this generalization, the predicted quartz geothermometer temperatures for the East Mesa test wells are in close agreement with their measured temperatures of 174 and 126°C. The recovery curves for Well 56-19, however, display flat minimums where concentrations are in agreement with chalcedony equilibrium. This occurs despite the abundant quartz in the East Mesa reservoir rock.

4.4.2 Na/K. Temperature-induced shifts in the Na/K and Na/Ca ratios of a fluid co-existing with alkali-bearing alumino-silicates have been predicted by theory and empirical data (e.g., Fournier and Truesdell, 1973). As shown in Figure 4.9, these shifts occurred in the fluid injected into Well 56-19. The Na-K-Ca (-Mg) geothermometer temperatures (Fournier and Truesdell, 1973; Fournier and Potter, 1979) were calculated from chemical analyses of the recovered fluid. Although these predicted temperatures are not valid due to the precipitation of calcite during the tests (Fournier and Truesdell, 1973), the similarity between the predicted and measured temperatures demonstrates that the ion ratio shifts were of proper magnitude and direction for decreasing fluid temperatures.

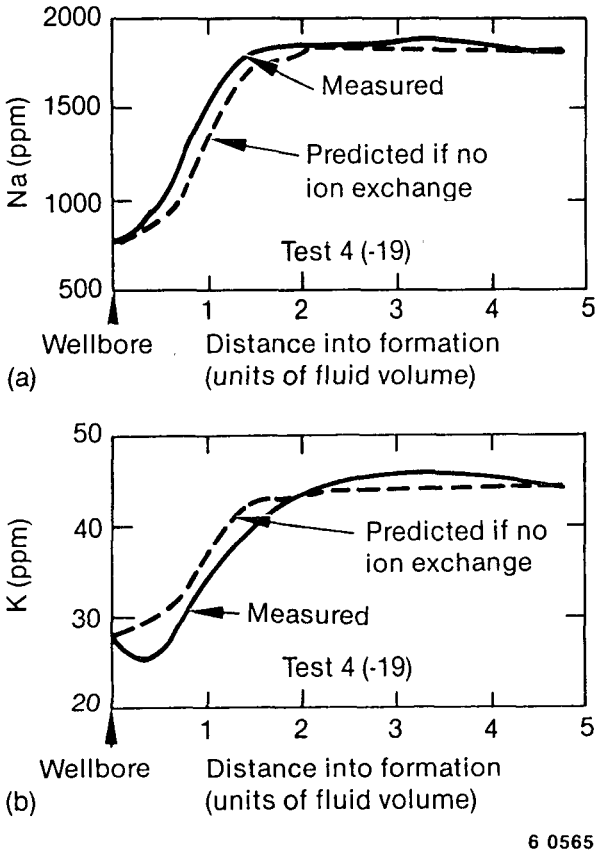

Figure 4.9 Recovery curve contrasting the behavior of Na and K in Well 56-19. See Figure 4.7 and text for explanation.

4.5 Summary

The chemical behavior and movement of injected fluids are a vital concern to geothermal operators. This behavior cannot be determined by equilibrium analysis, as shown by the metastable precipitation that occurred during the East Mesa injection tests. The only method of tracking the fluids and measuring subsurface precipitation, dissolution, and ion exchange is by referencing fluid concentrations to a chemical tracer. The chemical tracers currently in use by the geothermal industry are largely inadequate. They are either unstable, inaccurate, or clumsy to use.

The current program at UURI is designed to develop and test new tracers. The fluorinated and sulfonated hydrocarbons appear to be superb candidates. To date, four compounds have been tested which are more stable than the organic dyes currently used by the geothermal industry. In addition, the stabilizing and destabilizing effects of the geothermal environment on the organic dye fluorescein have been identified and quantified.

Much more laboratory testing is required to determine the stabilities and assess the high-temperature properties of the fluorinated and sulfonated hydrocarbons. As the characteristics of these hydrocarbons become better understood, it will become possible to design and test new species for specific applications. Bench tests, however, can only approximate the actual conditions occurring in the geothermal reservoir. Once the basic data is obtained, field tests of these tracers will be required to confirm their behavior.

4.6 References

M. C. Adams, "Tracer Stability and Chemical Changes in an Injected Geothermal Fluid During Injection-Backflow Testing at the East Mesa Geothermal Field," *10th Workshop on Geothermal Reservoir Engineering, Stanford University, 1985*, pp. 247-252.

R. O. Fournier, "Application of Water Chemistry to Geothermal Exploration and Reservoir Engineering," in Rhybach, L., and Muffler, L. J. P.: *Geothermal Systems: Principles and Case Histories*: New York: John Wiley & Sons, 1981, pp. 109-144.

R. O. Fournier and R. W. Potter, II, "Magnesium Correction to the Na-K-Ca Chemical Geothermometer:" *Geochim. Cosmochim. Acta, 43*, 1979, pp. 1543-1550.

R. O. Fournier and A. H. Truesdell, "An Empirical Na-K-Ca Geothermometer for Natural Waters:" *Geochim. Cosmochim. Acta, 37*, 1973, pp. 1255-1275.

J. S. Gudmundsson, et al. "Injection and Tracer Testing in Svartsengi Field, Iceland" *Proceeding of the Sixth N. Z. Geothermal Workshop, 1984*, pp. 175-180.

D. E. Michels, "Disposal of Flashed Brine Dosed With $CaCO_3$ Scale Inhibitor; What Happens When the Inhibitor is Exhausted," *Ninth Workshop on Geothermal Reservoir Engineering, Stanford University*, 1983, pp. 317-321.